Dynamics of phytoplankton productivity and exopolysaccharides (EPS and TEP) pools in the Seine Estuary (France, Normandy) over tidal cycles and over two contrasting seasons

Morelle Jérôme [1, 2], Schapira Mathilde [3], Claquin Pascal [1, 2, *]

[1] Normandie Université, Université de Caen-Normandie, Esplanade de la paix, F-14032 Caen, France
[2] UMR BOREA (CNRS-7208, IRD-207, MNHN, UPMC, UCBN), Esplanade de la paix, F-14032 Caen, France
[3] Ifremer, LER/N, Avenue du Général de Gaulle, 14520 Port-en-Bessin, France

* Corresponding author : Pascal Claquin, email address : pascal.claquin@unicaen.fr

Abstract :

Exopolysaccharides (EPS) play an important role in the carbon flux and may be directly linked to phytoplankton and microphytobenthos production, most notably in estuarine systems. However the temporal and spatial dynamics of estuarine EPS are still not well understood, nor how primary productivity triggers this variability at these different scales.

The aim of this study was to investigate the primary productivity of phytoplankton and EPS dynamics in the Seine estuary over a tidal cycle in three different haline zones over two contrasted seasons. The other objectives was to investigate the origin of pools of soluble carbohydrates (S-EPS) and transparent exopolymeric particles (TEP) in phytoplankton, microphytobenthos or other compartments. High frequency measurements of productivity were made in winter and summer 2015. Physical and chemical parameters, biomass and EPS were measured at hourly intervals in sub-surface waters and just above the water sediment-interface.

Our results confirmed that high frequency measurements improve the accuracy of primary productivity estimations and associated carbon fluxes in estuaries. The photosynthetic parameters were shown to be strongly controlled by salinity and by the concentrations of suspended particle matter at the smallest temporal and at spatial scales. At these scales, our results showed an inverse relationship between EPS concentrations and biomass and productivity, and a positive relationship with sediment resuspension. Additionally, the distribution of EPS appears to be linked to hydrodynamics with the tide at daily scale and with the winter at seasonal scale. At spatial scale, the maximum turbidity zone played an important role in the distribution of TEP.

Our results suggest that, in the Seine estuary, between 9% and 33% of the S-EPS pool in the water column can be attributed to phytoplankton excretion, while only 0.4%–1.6% (up to 6.14% in exceptional conditions) originates from the microphytobenthos compartments. Most EPS was attributed to

remobilization of detrital carbon pools in the maximum turbidity zone and in the sediment or allochthonous origin.

Highlights

► Accurate estimation of primary productivity in estuaries requires frequent measurements. ► An inverse relationship found between EPS concentrations and biomass and productivity. ► Only a minor fraction of the EPS pool was directly attributed to primary production. ► TEP concentration was strongly controlled by hydrodynamics.

1. Introduction

Located at the interface between the land and marine environments, estuaries provide economic, cultural and ecological benefits to communities (Viles and Spencer 1995; Higgins et al. 2010; Barbier and Hacker 2011). Estuaries are strategic areas for human activities but are also vital for wildlife, as they provide a wide variety of habitats for nesting and feeding (Ayadi et al. 2004; Kaiser 2011). Long-term management of estuarine ecosystems is currently seriously threatened by anthropogenic pressure and climate change (Porter et al. 2013), and requires a better understanding of the structure and function of the organisms at the base of the food web. The estuarine food web is based on organic matter, which can be of autochthonous or allochthonous origin. Primary production by microalgae (i.e. phytoplankton and microphytobenthos) accounts for a large proportion of autochthonous production in many estuaries (Underwood and Kromkamp 1999; Cloern et al. 2014). Primary production in estuaries varies considerably in space and over time, making it difficult to scale up measurements (Shaffer and Onuf 1985). Indeed, estuaries are unique aquatic environments that receive inputs derived from freshwater outflows from rivers and mechanical energy from tides (Cloern 1991; Statham 2012). In addition to processes in open oceans that explain their variability, in estuaries, primary producer dynamics is the result of many processes on land, in the atmosphere, in the ocean and in the underlying sediments (Cloern 1996; Morse et al. 2014). Many of these processes fluctuate over a wide range of timescales and the geographical position of each estuary characterizes the relative strength of these processes operating at annual, seasonal, monthly, daily and even at event timescales (Cloern and Jassby 2010; Parizzi et al. 2016).

Apart from photosynthesis of organic matter, a significant proportion of primary production is released as extracellular polysaccharides (EPS) (Passow 2002). EPS are mainly made up of a free fraction of soluble carbohydrates (S-EPS) (Underwood et al. 1995) composed of galactose and glucuronic acid (De Brouwer et al. 2002), but also of a particle fraction in the form of transparent exopolymer particles (TEP), mainly composed of fucose and rhamnose (Fukao et al. 2009). These exopolymers play an important role in aggregation processes, particle sedimentation and carbon fluxes in aquatic ecosystems (e.g. Passow et al. 2001; Bhaskar & Bhosle 2005). Moreover, the production of EPS allows the creation of microenvironments in which cells are protected from rapidly changing

80 environmental conditions, toxins, grazing, and even digestion (Decho 2000). In estuarine systems, EPS

81 have been shown to account for a large proportion of the colloidal organic carbon pool in the water

82 column (Annane et al. 2015) and high concentrations of TEP have been found in the maximum turbidity

83 zone (MTZ) of estuaries where suspended particle matter (SPM) accumulates (Malpezzi et al. 2013).

84 However, most research on EPS in estuaries has focused on their production by microphytobenthic

85 communities and only a few authors have studied EPS and TEP dynamics in the estuarine water column

86 (Wetz et al. 2009; Annane et al. 2015). As a result, the link between phytoplankton primary production

87 and the concentration of exopolymers in estuaries remains to be explored.

88 In estuaries, in addition to temperature and light, factors that potentially control primary production

89 are forced by tide variability and also by river runoff and nutrient inputs (Sun et al. 2012). At a small

90 scale, tidal regimes play a fundamental role in phytoplankton dynamics, as the movement of water

91 masses causes notable variations in salinity, and in SPM and nutrient concentrations (Monbet 1992;

92 Jouenne et al. 2007; Gameiro and Brotas 2010). Moreover, a strong salinity gradient in the estuary can

93 profoundly influence the distribution, dynamics and production of phytoplankton, which include

94 riverine, coastal and estuarine taxa (Muylaert et al. 2009). At seasonal scales, in temperate estuaries,

95 phytoplankton dynamics are characterized by higher freshwater species biomass during the high flow

96 period (i.e. winter) and high neritic diatom biomass during the low flow period (i.e. summer) (Cloern et

97 al. 1985; Alpine and Cloern 1992). In sum, phytoplankton productivity can vary considerably over a

98 wide range of scales, which, in turn, can strongly affect the biogeochemical functioning of the estuary.

99 Despite the need to better understand the dynamics of phytoplankton and primary production at these

100 different scales, only a few studies have addressed the variability of phytoplankton primary production

101 over a tidal cycle (Cloern 1991; Desmit et al. 2005). In this context, it is vital to investigate the factors

102 that control photosynthetic processes and carbon excretion by phytoplankton in estuaries.

103 Assessing small-scale temporal variability, such as the variability expected over a tidal cycle, requires

104 high frequency measurements. The Pulse Amplitude Modulated (PAM) fluorometry method, based on

105 the measurement of variation in fluorescence of the photosystem II (PSII), provides high frequency

106 measurements of photosynthetic parameters (Kromkamp and Forster 2003). While this method does not

107 directly measure the incorporation of photosynthetic carbon (Kolber and Falkowski 1993; Barranguet

108 and Kromkamp 2000), it enables monitoring of the dynamics of photosynthetic parameters directly

109 linked to carbon incorporation (Claquin et al. 2004; Napoleon et al. 2012).

110 The present study was conducted along the macro-tidal part of the Seine estuary, which forms the

111 biggest outflow into the English Channel. Given the variability of physical forcing in estuaries, the aim

112 of this work was to investigate the dynamics of EPS (S-EPS and TEP) in the water column and

113 phytoplankton primary productivity at appropriate temporal scales. Our specific objectives were to (1)

114 study the relationships between short-term EPS dynamics and phytoplankton primary productivity over

115 tidal cycles, (2) assess their variability along the salinity gradient, (3) explore these relationships over

116 two contrasted seasons: high flow/winter (February) and low flow/summer (July) and, finally (4) to

117 estimate the potential relative contribution of autochthonous phytoplankton primary production and

118 microphytobenthic productive mudflats, to the EPS pool in a temperate estuary.

119

120 **2. Methods**

121 **2.2. Study site**

122 The Seine River and its estuary drain an area of 76,260 km^2. After Paris, the river flows northwest and

123 drains into the English Channel. Located 202 km from Paris (the kilometric scale of the Seine River is

124 set at 0 km in the center of Paris), the weir at Poses represents the upper limit of tidal propagation of the

125 Seine estuary (Fig. 1). The annual mean discharge of the river measured at Poses is 436 m^3/s. During

126 the sampling year, the high flow period extending from January to May with a mean discharge of 750

127 m^3/s and values reaching 1,240 m^3/s and a mean discharge of 245 m^3/s during low flow period (Data

128 GIP Seine-Aval, 2008; 2011). Salinity ranges between (i) 0.5 and 5 in the oligohaline part, (ii) 5 and 18

129 in the mesohaline part, (iii) 18 and 30 in the polyhaline part, and (iv) salinity is higher than 30 in the

130 euhaline part of the Seine estuary. The Seine estuary is a macrotidal estuary, whose tidal amplitude

131 ranges from 3 to 7 m at Honfleur and from 1 to 2 m at Poses. The mean residence time in the estuary

132 ranges from 17 to 18 days for a discharge of 200 m^3/s at Poses and from 5 to 7 days for a discharge of

133 1,000 m^3/s (Brenon and Hir 1999; Even et al. 2007). The tide in the Seine estuary is characterized by

134 flattening at high tide that lasts for more than 2 hours due to the deformation of the tidal wave during

135 propagation at shallow depths (Brenon and Hir 1999; Wang et al. 2002). The flow is asymmetric in

136 favor of the flood and this trend increases when the tide propagates up the estuary (Le Hir et al. 2001).

137 Water temperatures range from 25 °C in summer to 7 °C in winter with differences of less than 1 °C

138 along the longitudinal axis and a weak vertical gradient (Data GIP Seine-Aval, 2008; 2011). The estuary

139 is characterized by the formation of a maximum turbidity zone (MTZ) containing up to 2 g/L of SPM,

140 usually located between Honfleur and Tancarville. However, depending on the intensity of the tide and

141 river discharge, the MTZ may move upstream, and, during winter flood events, the MTZ may be

142 flushed out into the Seine Bay (Etcheber et al. 2007; Garnier et al. 2010).

143

144 **2.2. Sampling strategy**

145 *Water column sampling*

146 Sampling was conducted in February (winter – high flow period) and July (summer – low flow

147 period) 2015 onboard the vessel "*Côtes de la Manche*". During both periods, sampling was conducted

148 under similar tidal conditions (i.e. the tidal range and the highest tidal elevation during daylight were

149 similar), at three sites distributed along the salinity gradient (Fig. 1): in the euhaline part at the river

150 plume (La Carosse - sampled on February 3 and July 18), in the mesohaline zone (Fatouville - sampled

151 on February 4 and July 20) and in the oligohaline zone (Tancarville - sampled on February 5 and July

152 17). Sampling was conducted during daylight over a tidal cycle (i.e. 12 hours) at each of the three sites

153 and during both campaigns. Photosynthetic parameters were measured in the surface water at five-

154 minute intervals (i.e. 12 measurements/hour). Vertical salinity (Practical Salinity Scale), turbidity

155 (Nephelometric Turbidity Unit) and temperature (°C) profiles were performed hourly with a SBE 19-

156 plusVD CTD (Seabird) from the sub-surface to 1 m above the water-sediment interface (WSI). Water

157 was sampled from the sub-surface (i.e. 1 m) and 1 m above the WSI using a 5 L-Niskin bottle at hourly

158 intervals to measure hydrological (i.e. nutrients, suspended particular matter) and biological (i.e.

159 chlorophyll *a*, EPS concentrations) parameters.

160

162   Two other campaigns were conducted in September, 2014 and in April, 2015 at 15 sites distributed

163   throughout the Seine estuary mudflats (the labels and coordinates are provided in the results section -

164   Tab. 2) to access the microphytobenthos dynamics (Morelle *et al*, in prep). Each site was sampled

165   during the emersion period (more than one hour after the beginning of the exposure period and more

166   than one hour before the return flow) and three replicated squares (1 x 1 m) were chosen randomly at

167   each site. In each square, three cores (20 cm diameter × 1 cm deep) were taken. After being carefully

168   homogenized, the volume of substratum was determined by using cut syringes, split into flasks for

169   analyses. The concentrations of the EPS in the samples were measured.

170

171   **2.3. High-frequency measurements**

172   **2.3.1. Photosynthetic parameters**

173   In order to acquire high-frequency estimations of primary productivity, the maximum energy

174   conversion efficiency (or the quantum efficiency of photosystem II (PSII) charge separation, F_V/F_M)

175   was measured at 5-minute intervals using the flow through version of the WATER PAM (Waltz,

176   Effeltrich, Germany) (Schreiber et al. 1986). Water collected from the sub-surface was conducted

177   through a pipe to a thermally insulated dark reserve that maintained the sample close to the *in situ*

178   temperature. After 5 min of dark acclimation, which was sufficient for the oxidation of the Quinone A

179   (Q_A) pool in this highly turbid environment, a sub-sample was automatically transferred into the

180   measuring chamber. The sample was excited by a weak blue light (1 μmol photon.m^{-2}.s^{-1}, 470 nm,

181   frequency 0.6 kHz) to record the minimum fluorescence (F_0). The maximum fluorescence (F_M) was

182   obtained during a saturating light pulse (0.6 s, up to 4000 μmol photon.m^{-2}.s^{-1}, 470 nm), allowing all

183   the Q_A pool to be reduced. Fv/F_M was calculated according to the following equation (Genty et al.

184   1989):

185    $$\frac{F_V}{F_M} = \frac{(F_M - F_0)}{F_M} \qquad (1)$$

186   Samples were exposed to nine consecutive irradiances (*E*) ranging from 0 to 469 μmol photon.m^{-2}.s^{-1} in

187   winter and from 0 to 1 541 in summer, for a period of 30 s for each light step. These different light

7

188 ranges were chosen to properly estimate the photosynthetic parameters. Steady state fluorescence (F_S)

189 and maximum fluorescence (F_M') were measured. The effective quantum efficiency of PSII for each

190 irradiance was determined as follows (Genty et al. 1989) :

191 $$\frac{\Delta F}{F_M'} = \frac{(F_M' - F_S)}{F_M'} \qquad (2)$$

192 The relative electron transport rate (rETR, µmol electron/m^2/s) was calculated for each irradiance. rETR

193 is a measure of the rate of linear electron transport through PSII, which is correlated with the overall

194 photosynthetic performance of the phytoplankton (Juneau and Harrison 2005):

195 $$rETR(E) = \frac{\Delta F}{F_M'} \times E \qquad (3)$$

196 Samples were removed from the Niskin bottle in sub-surface water and close to the WSI at hourly

197 intervals. A sub-sample was placed in the measuring chamber of the cuvette version of the WATER

198 PAM (Waltz, Effeltrich, Germany) and F_V/F_M was measured as described above.

199

2.3.2. P versus E curves

201 To estimate the photosynthetic parameters, the rETR values were plotted against E and the mechanistic

202 model developed by Eilers & Peeters (1988) was applied to fit the data using SigmaPlot (Systat

203 Software) according to the equation (4) with a, b and c initially set to 3×10^{-5}; 0.06 and 111 respectively:

204 $$rETR(E) = \frac{E}{(aE^2 + bE + c)} \qquad (4)$$

205 After 200 iterations of fit per curve, the best a, b and c parameters were estimated by the software for

206 each rETR/E curve and the maximum photosynthetic capacity $rETR_{max}$ was calculated as follows:

207 $$rETR_{max} = \frac{1}{(b + 2\sqrt{ac})} \qquad (5)$$

208

2.4. Discrete measurements

2.4.1. Nutrients

211 To determine nutrient concentrations (PO_4^{3-}, NO_3^-, NO_2^-, NH_4^+ and $Si(OH)_4$), 100 ml water samples

212 were pre-filtered through a 48 µm Nylon Mesh (Sefar Nitex 03-48/31-102 cm; Open area %: 30)

213 directly from the Niskin bottle in order to already eliminate a major part of the particles (Aminot and

214 Kérouel 2004, 2007). For the measurement of silicate concentrations (Si(OH)$_4$), water samples were

215 subsequently filtered through 0.45 µm acetate cellulose membrane and stored at 4 °C until analysis. For

216 the measurement of dissolved inorganic nitrogen (i.e. DIN = NO_3^- + NO_2^- + NH_4^+) and phosphate

217 concentrations (PO_4^{3-}), water samples were stored directly at -20 °C. Samples were analyzed within one

218 month after field collection with an auto-analyzer (Technicon III) following standard protocols (Aminot

219 and Kérouel 2007; Hydes et al. 2010). The limits of quantification were 0.2 µM for silicates, 0.1 µM for

220 nitrates, 0.02 µM for nitrites, 0.04 µM for phosphates and 0.1 µM for ammonia.

221

222 **2.4.2. Suspended particulate matter**

223 Surface and bottom water samples were collected from the Niskin bottle at hourly intervals over the

224 12 h tidal cycle. Before the field campaign, Whatman GF/F glass microfiber 0.7 µm filters were

225 prepared and rinsed using the vacuum filtration system, dried at 50 °C for 24 h, and pre-weighed. A

226 known volume of the sampled water was filtered through the prepared filters using a glass tank on a

227 filter ramp connected to a pump. Filters were rinsed with distilled water to remove any remaining salt.

228 The concentration of total suspended solids (g/L) was then calculated by gravimetric determination after

229 air-drying the filters for 24 h at 50 °C and weighing on a high precision Sartorius scale. This method

230 ensured a precision of 0.0001 g/L for the lowest SPM concentrations (Verney et al. 2009).

231

232 **2.4.3. Phytoplankton biomass**

233 Phytoplankton biomass was assessed through chlorophyll *a* (chl*a*) concentrations. Samples (30 to 500

234 ml) were filtered in triplicate, through glass fiber filters (Whatman GF/F: 0.7 µm pore size and 47 mm

235 diameter) and immediately frozen at -20 °C until analysis. In the laboratory, pigments were extracted in

236 10 mL of 90% (v/v) acetone, for 12 h at 4 °C in the dark. After centrifugation (3000 g, 4 °C, 10

237 minutes), the chl*a* concentration (µg/L) was measured on extracts according to the fluorometric method

238 of Lorenzen (1966) and using a Turner Trilogy fluorometer (Turner Designs, Sunnyvale, California,

239 USA).

2.4.4. Extracellular polymeric substances

Water column pools

The concentration of TEP was determined using the colorimetric method described by Claquin et al. (2008) adapted from Passow and Alldredge (1995). Briefly, 15 to 50 ml samples were filtered onto 0.4 µm polycarbonate Isopore membrane filters (Millipore) and stored at -20 °C until analysis. Particles retained on the filters were stained with 5 ml of 0.02% Alcian blue (Sigma) in 0.06% acetic acid (pH 2.5). After centrifugation at 3500 g for 30 min, the supernatants were removed and the filters were centrifuged several times with 5 ml of MilliQ water until all excess dye was completely removed from the pellet. After one night of drying in a sterilizer at 50 °C, 6 ml of 80% H_2SO_4 were added and 2 hours later the absorption of the supernatant was measured using a spectrometer at 787 nm. Alcian blue absorption was calibrated using a solution of Xanthan gum (XG) as a standard. TEP concentrations are expressed in µgXGeq/L. Subsequently, to estimate the TEP pool in the water column, the TEP concentrations were converted into carbon (mgC/L) using a coefficient of 0.70 (Engel and Passow 2001; Claquin et al. 2008).

Carbohydrate content was measured using Dubois's method (Dubois et al. 1956). Briefly, the filtrates of TEP filters were considered as colloidal EPS (S-EPS). High and low molecular weight EPS was extracted by incubating the samples in ethanol (70% f.c.) for 16 hours at −20 °C. Samples were centrifuged at 3000 g, for 30 min at 4 °C. Low molecular weight EPS was collected in the supernatant and discarded. The pellet containing high molecular weight EPS was dried at 50 °C overnight. The dried samples were re-suspended in 1 ml distilled water. Next, 50 µL of 5% phenol and 250 µL sulfuric acid were added to 50 µL of the extract, and vortexed. Absorption was read after 30 min with a FlexStation plate reader (Molecular Devices) at 485 nm, using glucose (G) as a standard for the calibration curve. S-EPS concentrations are expressed in µgGeq/L.

Intertidal sediment pools

Fresh sediments were treated immediately on return to the laboratory to avoid any cell disruption or contamination of EPS extracts by chrysolaminarin stored in the vacuoles (Chiovitti et al. 2004; Takahashi et al. 2009). Following Orvain et al. (2014), microphytobenthic EPS was extracted from 5 ml of fresh sediment placed in 15 ml centrifugation tubes with 5 ml of 0.2 μm filtered and sterilized artificial sea water. After one hour of incubation in artificial seawater, tubes were mixed and centrifuged at 4 °C, 3000 g for 10 min. Supernatants containing the colloidal fraction were collected in a new centrifugation tube and stored frozen (−20 °C) until analysis. The method described above for phytoplanktonic S-EPS was used. Each EPS concentration was first expressed as a function of the volume of fresh sediment (mgGeq/L) and was then converted into contents (mgGeq/gDW) by using the volumetric mass (in g/L) and into surface units (mgGeq/m^2) by using the dry bulk density (in kg/m^3) and considering a core depth of 1 cm. The chl*a* data, which were also measured during these campaigns using the Lorenzen method (1966), were used to express the S-EPS:chl*a* ratio in mgGeq/mgchl*a*.

2.5. Data analysis

P-E curves & Spearman correlations were performed using the SigmaPlot (Systat software) and linear & multiple regressions using the R software (R Development Core Team) to investigate correlations between parameters at each site, in the two seasons, and at both depths. Significant correlations were accepted when the p-value was < 0.05. A principal component analysis (PCA) was performed using the "FactoMineR" package in R on data collected from the sub-surface and close to the WSI at hourly intervals at the three sampling sites in the two sampling periods. The data were not transformed before analyses.

3. Results

3.1. Spatial and temporal dynamics of the water column along the salinity gradient

The temperature, salinity and nutrient dynamics are characteristic of North European estuaries (Fig. S1 & S2). The main points regarding these parameters are the higher temperature (> 18 °C) and the lower river flow in summer (< 226 m^3/s) versus winter (temperature < 7°C and flow > 1110 m^3/s). In

11

293 both seasons, the salinity gradient ranged between 0.01 and 32.37, extended upstream up to Tancarville

294 in summer and up to Fatouville in winter. In summer, despite the low river flow, nutrient concentrations

295 remained high (between 9.17 and 413.54 µM for [DIN], between 5.22 and 160.20 µM for [Si] and,

296 between 0.36 and 4.17 µM for [P]) and were not limiting for phytoplankton growth during this period.

297 [DIN] and [Si], were closely linked to freshwater inputs and decreased from upstream to downstream.

298 In contrast, [P] was positively correlated with the tidal height and the highest concentrations were

299 recorded in the mesohaline part of the estuary.

300 The highest SPM concentrations were recorded close to the WSI, at Fatouville during winter, and at

301 Tancarville during summer (Tab. 1). The sampling site La Carosse displayed characteristics of marine

302 waters with very low SPM concentrations. At Fatouville in winter, peaks of SPM were recorded close to

303 the WSI at the beginning of the high tide and during the ebb (fig. S3), whereas very low SPM

304 concentrations were observed during the high tide slack. A very similar pattern was observed in

305 summer, with high SPM concentrations recorded close to the WSI at the beginning of the high tide and

306 at low tide. At Tancarville, a peak was recorded at both depths during the ebb in winter, and during low

307 tide in summer. These observations suggest that SPM concentrations were closely linked to

308 resuspension of bottom sediments triggered by tidal currents rather than to inputs from the watershed.

309 Nevertheless, the pattern of variation in SPM concentrations in surface was closely linked to the

310 dynamics of SPM observed close to the WSI. This observation suggests that resuspension of sediment

311 by tidal currents has an impact on the entire water column. Our results also suggest that the MTZ was

312 located between Fatouville and Tancarville in winter, and upstream from Tancarville in summer.

313

314 **3.2. Discrete measurements of chl*a* biomass and photosynthetic parameters**

315 The chl*a* concentrations were low in winter (Tab. 1) with minor variations at La Carosse and

316 Tancarville (Fig. 2). Only three peaks were recorded close to the WSI at Fatouville associated with

317 SPM dynamics (during the flood, the high tide slack and the ebb). In summer, at La Carosse, an

318 increase was recorded during the flood at both depths but the increase was bigger at the surface. At

319 Fatouville, chl*a* concentrations were low close to the WSI except for a peak at low tide slack. In surface

320 waters, values were low at low tide slack but increased considerably from the flood to the high tide

321 slack. At Tancarville, the chl*a* concentrations decreased during the flow and increased during the ebb at

322 both depths.

323 At La Carosse, despite low chl*a* in winter, F_V/F_M values were high (Tab. 1). The highest F_V/F_M values

324 were recorded at both depths during tide slack. However, marked variations were recorded over the tidal

325 cycle (Fig. 2), two reductions were recorded during the flood and during the ebb at both depths. At

326 Fatouville, F_V/F_M values were low and remained constant throughout the day. At Tancarville, two

327 reductions were recorded, one during the flow and the other at the beginning of the ebb. Despite the

328 high chl*a* concentrations in summer, F_V/F_M were lower than in winter. At La Carosse, at both depths,

329 F_V/F_M increased during the flood, decreased during high tide and increased during the ebb. At

330 Fatouville, F_V/F_M were closely linked to the dynamics of the tide characterized by a decreasing trend

331 during the ebb followed by an increase with the flow to reach maximum values during high tide. At

332 Tancarville, F_V/F_M values were very low with high variability over the tidal cycle.

333

334 **3.3. High frequency measurements of photosynthetic parameters**

335 Primary productivity estimated using high frequency $rETR_{max}$ (µmol electron/m^2/s) measurements

336 showed a high degree of variability at very small temporal scale (5 min) compared with hourly

337 observations (Fig. 3). In winter, productivity values were low (Tab. 1). At La Carosse, $rETR_{max}$

338 decreased during the flow, increased during high tide and decreased at the beginning of the ebb

339 followed by marked variability of the values. At Fatouville, $rETR_{max}$ increased during the flow, when

340 currents were at their maximum, and decreased during tide slacks. At Tancarville, despite the high

341 degree of variability, the $rETR_{max}$ remained close to a mean value of 30.16 ± 6.42 µmol electron/m^2/s.

342 In summer, $rETR_{max}$ values were higher than in winter throughout the salinity gradient (Tab. 1). At La

343 Carosse, the dynamics of phytoplankton productivity increased from low tide to half the flow.

344 Thereafter a decrease was observed during the high tide before a slight increase at the beginning of the

345 ebb. At Fatouville, productivity mirrored tidal dynamics but with a time lag of approximately three

346 hours. At Tancarville, an increase in productivity from the morning low tide to high tide was followed

347 by a decrease from high tide to the evening low tide.

348

349 **3.4. Extracellular polymeric substances.**

350 **3.4.1 Transparent exopolymeric particles (TEP)**

351 At each site, TEP concentrations ([TEP], mgXGeq/L) were higher close to the WSI than in sub-

352 surface waters (Tab. 1) and [TEP] peaks were mostly recorded during flows (Fig. 4). In winter, at La

353 Carosse, three peaks were recorded close to the WSI: two during the high tide, mirroring the tide

354 dynamics, and one at the end of the ebb. In sub-surface waters, a peak was recorded at the beginning of

355 the flow and an increasing trend was recorded during the ebb. At Fatouville, high variability was

356 observed close to the WSI with values increasing both during the flow and the ebb. At the surface, the

357 same dynamics were observed but with lower values. At Tancarville, some [TEP] peaks were also

358 observed during the flow and the ebb at both depths. During summer, [TEP] variations at La Carosse

359 were weak despite two small peaks close to the WSI recorded during the flow. Upstream, at Fatouville

360 and Tancarville, high peaks were recorded during low tide at both depths, small peaks were also

361 recorded at high tide at both these sites. Thus, during the campaigns, it appears that between 0.36 and

362 48.08 mgC/L and a mean of 5.89 mgC/L were available for the trophic network in the form of TEP.

363 The TEP:chl*a* ratios were higher in winter than in summer (Tab. 1). Some decreasing trends in the

364 TEP:chl*a* ratio were recorded at high tide slacks in the sub-surface water at La Carosse in both seasons

365 and in summer at Fatouville at both depths with an inverse dynamics with respect to the tide (Fig. S4).

366 Some negative peaks were also recorded at the end of the high tide slacks.

367

368 **3.4.2 Soluble carbohydrates (S-EPS)**

369 *Water column pools*

370 Despite high variability, the S-EPS concentrations ([S-EPS]) were higher close to the WSI than in

371 sub-surface waters and in winter than in summer (Tab. 1). Some peaks were recorded at both depths

372 mainly during the reverse flows (before and after the tide slacks) (Fig. 5). The highest peaks and the

highest variability were observed close to the WSI. In winter, high variability was recorded at Fatouville during the ebb. In summer, at La Carosse, highly variable values were recorded during low tide especially in sub-surface waters whereas inverse patterns were observed at the two sampling depths. At Fatouville, [S-EPS], the same patterns were observed at both depths with decreasing values at slack tides and peaks during the flows. At Tancarville, [S-EPS] were characterized by a marked increase close to the WSI at high tide and high variability during the ebb.

EPS:chl*a* ratios presented some peaks at both depths (Fig. S5). In winter at La Carosse, a strong peak was observed close to the WSI at the end of the ebb. In summer, the highest values were recorded close to the WSI during the ebb. In winter at Fatouville, EPS:chl*a* ratios in sub-surface waters increased during the high tide and were variable at the beginning of the ebb, while close to the WSI, some peaks were recorded during the tide slacks and the ebb. In summer, a strong peak was recorded in sub-surface waters during the flow, followed by a marked decrease during the high tide slack. Close to the WSI, a peak was recorded at the end of the ebb. In winter at Tancarville, an increase in the EPS:chl*a* ratio was recorded at the end of the ebb close to the WSI. In summer, values were low at both depths during the low tide and the flow. Two peaks were recorded close to the WSI during the high tide slack and the ebb and one peak was recorded in sub-surface waters at high tide.

Intertidal sediment pools

S-EPS concentrations on the Seine estuary mudflats also displayed high variability among the 15 sites sampled (Tab. 2; Morelle *et al*, in prep). Values ranged between 61.02 and 526.04 mgGeq/m^2 also varied between seasons with a higher mean value in September (310.81 ± 129.61 mgGeq/m^2) than in April (157.06 ± 66.16 mgGeq/m^2). In contrast, the EPS:chl*a* ratios were often higher in April (19.74 ± 24.08 mgGeq/mgchl*a*) than in September (9.50 ± 8.93 mgGeq/mgchl*a*).

3.5. Relationships between biological parameters and environmental variables

Principal component analyses (PCA) were performed on the data set to explore the relationships between biological and abiotic parameters (Fig. 6). The 1st and 2nd components explained 65.26% of the

15

total inertia while the 1st and the 3rd dimensions explained 59.40% of total inertia (Tab. 3). The first

principal components (PC1; 41% of variance) formed a typical estuarine axis with parameters related to

the inflow of marine waters such as salinity (32%) on the left hand side of axis 1, and parameters related

to freshwater inputs, such as Si (23%) and DIN (33%) concentrations on the right hand side of axis 1.

The second principal component (PC2; 24%) was strongly influenced by factors related to seasonal

changes such as PAR (38%) and temperature (48%). The third principal components (PC3; 18%) was

related to P concentrations (58) and SPM (21%). The chl*a* concentrations (chl *a*) were positively

correlated with temperature (Spearman correlation coefficient (SCC): 0.59; p< 0.001; n=150) and PAR

(SCC: 0.42; p< 0.001; n=150). In the same way, productivity was positively correlated with temperature

(SCC: 0.60; p< 0.001; n=75) and PAR (SCC: 0.66; p< 0.001; n=75). Indeed, the high temperatures and

high solar irradiance in summer provide the best environmental growth conditions for phytoplankton.

The chl*a* was negatively correlated with P concentration (SCC: -0.20; p< 0.05; n=150) as confirmed by

their position in the $1^{st}/3^{rd}$ dimensions of the PCA (Fig. 9). F_V/F_M was positively correlated with salinity

(SCC: 0.22; p< 0.01; n=150), and negatively correlated with temperature (SCC: -0.27; p< 0.01; n=150),

and SPM (SCC: -0.15; p=0.06; n=150) concentrations. [TEP] were positively correlated with SPM

(SCC: 0.17; p< 0.05; n=150). The [S-EPS], S-EPS:chl*a* and TEP:chl*a* ratios were negatively correlated

with temperature, PAR, chl*a* and productivity (SCCs: < -0.44; p< 0.001; n=150).

4. Discussion

4.1. Dynamics of biological parameters in the Seine estuary in relation with environmental parameters

Our study revealed high variability of photosynthetic parameters in the estuary, where small-scale

variability (i.e. 5 minutes) can be greater than variability at tidal scale (Fig. 3). Less frequent

measurements could thus easily result in over- or underestimation of these parameters, thereby

highlighting the complexity of estimating primary productivity in these dynamic ecosystems. Moreover,

variability appeared to be higher and more frequent before or after the low or the high tide at which time

16

426 turbulence and the concentrations of SPM generally reach maximum levels thereby preventing light

427 from penetrating and hence preventing photosynthesis.

428 　Even though variations in nutrient concentrations are known to play a major role in phytoplankton

429 dynamics in many ecosystems, in many estuaries, it has been shown that nutrients do not control

430 phytoplankton growth because they are largely in excess (Kromkamp et al. 1995; Cai et al. 2004).

431 However, in this study, P concentrations were negatively correlated with phytoplankton biomass and

432 productivity (Fig. 6). This could be the result of the consumption of P by phytoplankton but P

433 concentrations within the estuary (> 0.62 µmol/L for all the samples) remained higher than those

434 usually observed during the same period in the Seine Bay (i.e. ≤ 0.04 µM) where phytoplankton grow

435 easily. Moreover, previous studies have shown that P does not limit phytoplankton growth in the Seine

436 estuary (Némery and Garnier 2007; Passy et al. 2016). Phosphate has a strong affinity for sorption and

437 desorption reactions with SPM, which create high fluxes and is an important source of dissolved P in

438 the MTZ (Némery and Garnier 2007). Therefore, this negative relationship may rather be related to a

439 positive relationship between P and SPM that reduces light penetration into the water column, and

440 consequently results in low phytoplankton biomass and productivity. Thus, like in many temperate

441 estuaries, phytoplankton productivity in the Seine estuary is mainly controlled by light availability.

442 　The physiological status of the cells (F_V/F_M) was low within the MTZ during both study periods (Tab.

443 1). This could be explained by the intense resuspension of dead cells and SPM in this area, which

444 reduced light penetration, especially during the flow and ebb. Additionally, the physiological changes in

445 the phytoplankton caused by the contrast between freshwater outflow and marine water inflow have

446 been shown to cause physiological stress and cell lysis (Lionard et al. 2005; Servais and Garnier 2006;

447 Hernando et al. 2015). However, despite weak F_V/F_M, phytoplankton productivity levels in the MTZ

448 (Fatouville in winter and Tancarville in summer) were in the same order of magnitude as those

449 measured at the two other sites in the same season (Tab. 1). This result shows that photosynthetic

450 activity of living cells is possible in the MTZ despite the high level of stress. More surprisingly, F_V/F_M

451 values were higher close to the WSI than in sub-surface waters. These results suggest that, despite the

452 high concentrations of SPM close to the WSI and the subsequent reduction in light penetration into the

17

453 water column, phytoplankton cells were able to survive and even to maintain a high physiological

454 status. The deep water layer corresponds to marine water with a residence time ranging from 5 to 18

455 days (Brenon and Hir 1999; Even et al. 2007). This observation suggests that these photosynthetic cells

456 are able to rapidly return to a high productive status as soon as they access light. This result further

457 implies that organic matter in the bottom layer of the Seine Estuary is probably not only composed of

458 detrital matter but also of living phytoplankton cells. This observation may have major implications for

459 trophic transfer between pelagic and benthic organisms in this part of the estuary.

460   In winter, at spatial scale, phytoplankton biomass and productivity were higher in the oligohaline

461 zone (Tancarville) than in the euhaline zone (La Carosse) (Tab. 1). The winter season involves an

462 increase in freshwater discharge and can increase phytoplankton growth, as already observed in the

463 Godavari estuary (Sarma et al. 2009) and in the Chesapeake estuary (Adolf et al. 2006). The higher

464 productivity observed at Fatouville (MTZ) at low tide rather than at high tide (Fig. 3) suggests higher

465 primary productivity in fresh waters than in saline waters during this period. Different community

466 composition in these distinct water masses could explain this result. Indeed, in winter, high primary

467 production in freshwater has been reported in other estuarine systems (Servais and Garnier 2006;

468 Lehman 2007) where it was attributed to specific freshwater phytoplankton communities (Malpezzi et

469 al. 2013). The presence of cyanobacteria in the outer part of estuary could also explain the low level of

470 primary productivity measured in the oligohaline zone of the estuary in winter: cyanobacteria display

471 lower productivity than eukaryotic phytoplankton (Masojidek et al. 2001; Macintyre et al. 2002). PAM

472 measurements may have underestimated cyanobacteria productivity, as the blue light used in the present

473 study is weakly absorbed by the prokaryotic fraction of the phytoplankton (Glover et al. 1985; Suggett

474 et al. 2004). In addition, the F_V/F_M is known to be poorly estimated in cyanobacteria because of the state

475 transition processes (Campbell et al. 1998).

476   In summer, the low discharge enables upstream migration of marine and estuarine species (Josselyn

477 and West 1985), which could explain the high phytoplankton biomass observed close to the WSI at

478 Fatouville and Tancarville (Tab. 1). The high phytoplankton growth rate observed in the Seine river

479 plume led to an increase in productivity at La Carosse at the beginning of the flow (Fig. 3). During the

ebb, a decrease in productivity was observed, possibly the consequence of the increase in SPM and the subsequent reduction in light penetration, or potential damage to phytoplankton cells caused by the mechanical stress associated with strong hydrodynamics, as previously shown in other estuarine systems (Cloern et al. 1985; Servais and Garnier 2006). The highest primary productivity in summer was observed at Fatouville in the mesohaline zone (Tab. 1). At this site, primary productivity increased with the flow and decreased with the ebb (Fig. 3). This result suggests that phytoplankton growth occurred in the polyhaline zone between La Carosse and Fatouville where the concentrations of nutrients were still high and light still available, but not in the other zones.

4.2. Dynamics of EPS in the Seine estuary in relation with environmental parameters

It has already been shown that in very dynamic zones like estuaries, the distribution of TEP may be mainly controlled by environmental processes (Malpezzi et al. 2013). In the literature, TEP production has been frequently associated with nutrient stress (Corzo et al. 2000; Passow 2002). However, the estuarine systems are not nutrient limited, but high values of [TEP] were recorded (Tab. 1). This result confirms that TEP production can be high in nutrient replete conditions as already reported (Claquin et al. 2008; Pedrotti et al. 2010). Thus in the present study, it is possible that the [TEP] dynamics were not associated with nutrient limitation as often cited in the literature but with other processes such as temperature (Claquin et al. 2008) or turbulence intensity (Pedrotti et al. 2010).

The [TEP] measured in the Seine estuary during this survey (0.52 - 68.7 mgXGeq/L; Tab. 1) was higher than those reported in the literature, which never exceeded 11 mgXGeq/L (Passow 2002), 2.82 mgXGeq/L (Malpezzi et al. 2013), 14.8 mgXGeq/L (Radić et al. 2005) or 1.54 mgXGeq/L (Annane et al. 2015). Villacorte et al. (2015) investigated the difference in measurements in TEP (> 0.4 µm) and TEP with $TEP_{precursors}$ (<0.4 µm) and showed that [TEP] could represent about 11% of [TEP+$TEP_{precursors}$]. The high SPM concentrations (up to 2 g/L; Tab. 1) in some samples could have allowed the retention of the $TEP_{precursors}$ on the filters thereby partly explaining the very high values observed along the Seine estuary.

506   However, the positive relationship observed between [TEP] and SPM is in agreement with the widely

507   described role of TEP and EPS in particle aggregation and sedimentation processes (Passow 2002;

508   Thornton 2002). In estuaries, very high TEP concentrations have also been measured in association with

509   SPM in the MTZ and shown to account for a significant proportion of the POC in MTZ (Malpezzi et al.

510   2013; Annane et al. 2015). Indeed, because of their sticky properties (Engel 2000; Passow 2002), TEP,

511   associated with a strong salinity gradient and turbulence, promote the aggregation and sedimentation of

512   organic and mineral particles especially within the MTZ and hence influence the dynamics of POM and

513   SPM in the estuary. These processes could explain the distribution of TEP at spatial scale with high

514   concentrations recorded in the MTZ (Tab. 1). In addition, the mixing of freshwater and seawater affects

515   the concentration of some ions and cations responsible for salinity, which could play a major role in the

516   crosslinking of polysaccharides to form gel-like particles such as TEP (Bar-Zeev et al. 2015). This form

517   of TEP formation could reinforce the high [TEP] recorded in the estuary and explain part of the positive

518   relationship with SPM associated with a negative relationship with salinity (Fig. 6). Indeed, due to

519   stratification, the mixing of fresh and salt water is particularly intense in the low salinity zone that

520   promotes TEP at MTZ level.

521   At the daily scale, the high concentrations of TEP in the Seine estuary were mainly linked to tidal

522   flows and mainly recorded within the Seine river plume or the MTZ (Fig. 4), which are both subject to

523   high levels of turbulence leading to resuspension of exopolysaccharide-rich particles from the sediment.

524   At the seasonal scale, the highest concentrations of TEP were recorded during the winter period

525   throughout the salinity gradient (Tab. 1). This seasonal dynamics could be related to higher

526   hydrodynamics in winter, triggered by the combination of strong currents along the estuary during this

527   high flow period and the frequent stormy and windy conditions in this season. These strong

528   hydrodynamics cause higher levels of sediment resuspension from the WSI in winter than in summer.

529   The S-EPS distribution in the Seine estuary could also be linked to environmental processes. At daily

530   scale, no clear pattern emerged from the S-EPS concentration due to the high variability of the values

531   measured (Fig. 5). However, some peaks were observable both in sub-surface waters and close to the

532   WSI especially at the beginning or end of the flows. This observation suggests that the distribution of S-

EPS could also be related to resuspension especially before or after tide slacks. At the seasonal scale, the S-EPS were also higher in winter and highest close to the WSI (Tab. 1) thus possibly reinforcing the influence of environmental parameters on S-EPS distribution in the Seine estuary. However, at spatial scale, the concentrations of S-EPS were not linked to the MTZ, like the TEP concentrations, and no relationship was observed with the SPM concentration. This observation suggests that the adsorption characteristics of those S-EPS were lower than TEP. In comparison with TEP, S-EPS easily dissolves in water so their adsorption in the water column could be limited and their concentration more closely linked to biological parameters (De Brouwer et al. 2002). Despite the fact that environmental processes play an important role in distributions of both TEP and S-EPS in the Seine estuary, these processes are mainly produced by biological organisms and the concentrations of those polysaccharides in relation to biological parameters remain to be investigated.

4.3. Dynamics of EPS in the Seine estuary in relation with biological parameters

The TEP is mainly produced by phytoplankton and significant correlations between TEP concentrations and phytoplankton dynamics have already been described (Hong 1997; Beauvais et al. 2003; Radić et al. 2005; Wurl and Holmes 2008; Klein et al. 2011). Nevertheless, some studies found no direct correlation between the TEP fraction and chl*a* (Garcia 2002; Corzo et al. 2005). In the present study, a negative correlation was found between TEP and chl*a* (Fig. 6). Our results are comparable with those of Chowdhury et al. (2016) and Klein et al. (2011), who reported low concentrations of TEP during maximum abundance of phytoplankton and higher concentrations during phytoplankton senescence which, in estuaries, is especially important in the MTZ. Moreover, our TEP:chl*a* ratios were inversely correlated with chl*a* and productivity. This observation suggests that the stress generated in the estuary leads to high levels of TEP excretion by the phytoplankton. This hypothesis is supported by the negative correlation between [TEP] and F_V/F_M. However, the TEP:chla ratios observed in this study (Tab. 1) are also high in comparison with those previously reported in the literature (Passow 2002; Klein et al. 2011). Therefore, the [TEP] may not be only linked to phytoplankton production. However, the TEP:chla ratios observed in this study (Tab. 1) are also high in comparison with those previously

reported in the literature (Passow 2002; Klein et al. 2011). Therefore, the [TEP] may not be only linked

to phytoplankton production. In strong hydrodynamic conditions, the high [TEP] in the MTZ may also

be attributed to the microbial loop activity. Indeed, it has been shown that the POM from the MTZ is

biodegraded by highly active heterotrophic bacteria that can also release TEP into the water column

(Azam et al. 1983; Middelburg and Herman 2007; Malpezzi et al. 2013). Moreover, significant

quantities of TEP could be derived from allochthonous inputs of organic matter that include high

concentrations of detrital material and heterotrophic bacteria (Heip et al. 1995).

S-EPS produced by phytoplankton are known to protect cells against digestive enzymes, toxic

substances (Wotton 2004), and osmotic stress (Liu and Buskey 2000), which is a major constraint in

estuaries. Additionally, S-EPS can be produced by phytoplankton in aiding in flotation process through

their threads and by reducing density (Wotton 2004). These potential roles of S-EPS could explain the

high concentrations observed in this study (Tab. 1) especially during flows (Fig. 5). In addition to chla

dynamics, changes in carbon excretion and photosynthetic parameters can may also be due to different

phytoplankton assemblages combined with water mass dynamics (Klein et al. 2011). However, no

relationship was found with the F_V/F_M, and S-EPS concentrations were negatively correlated with chl*a*

concentrations and productivity, which confirm results of previous studies (Passow 2002; Klein et al.

2011) showing that, in contrast to TEP, a large proportion of the S-EPS pools were not related to

phytoplankton dynamics.

4.4. Potential contribution of allochthonous primary producers to the S-EPS pool

Both groups of phototrophic microorganisms (phytoplankton and microphytobenthos) excrete S-EPS

for different reasons and in different ways. Due to the key roles played by EPS in epipelic diatom

dynamics in mobility and substratum adhesion, the S-EPS dynamics in ecosystems have often been

linked with microphytobenthos cells. However, in the Seine estuary the surface of mudflat during low

tide represents only 7.21% of the estuarine surface and no subtidal microphytobenthos community

exists because of the high level of turbidity and the depth (up to 18 m). Additionally, the mudflat is a

plane system and microphytobenthos are especially active during emersion during the daylight period

587   whereas the pelagic system is volumetric: in the Seine estuary for a mudflat surface of 7.6×10^6 m^2, the

588   water volume is 930×10^6 m^3 (on average between low and high tides).

589   We estimated potential S-EPS production by the microphytobenthic compartment using the data we

590   sampled in the intertidal zones (Morelle *et al*, in prep) and a microphytobenthic EPS production

591   coefficient estimated at 1.8 mgGeq/mgchl*a*/h (Wolfstein et al. 2002). Assuming a tidal emersion during

592   daylight of 6 hours per day and a maximum residence time of 18 days in the Seine estuary (Brenon and

593   Hir 1999; Even et al. 2007), the S-EPS pool originating from microphytobenthos represents 0.055 ±

594   0.054 mgGeq/L in the water column. The percentage of S-EPS originating from microphytobenthos

595   production could represent an average of 1.61% of the mean S-EPS pool measured during this survey.

596   In the same way, we estimated potential phytoplankton S-EPS production using a production coefficient

597   40% lower than microphytobenthos production (Goto et al. 1999), i.e. 1.08 mgGeq/mgchl*a*/h. The S-

598   EPS pool originating from phytoplankton represent 1.15 ± 1.54 mgGeq/L in the water column. On

599   average, the percentage of EPS originating from phytoplankton production could represent 33.62% of

600   the mean S-EPS pool measured during this survey. However, we used a maximum residence time of 18

601   days whereas in reality, the residence time ranged between 5 and 18 days. If we used the minimum

602   residence time of 5 days, the percentage would be 9.34% for the phytoplankton and 0.44% for the

603   microphytobenthos. In addition, if we consider that, in exceptional conditions, all the S-EPS pool

604   present on mudflats could be re-suspended in the water column each day, considering 5 to 18 days

605   residence time, the percentage of S-EPS from microphytobenthos production could represent from 1.70

606   to 6.14% of the mean S-EPS pool measured in the water column. Thus, we suggest that part of [S-EPS]

607   in the Seine estuary is not directly linked to primary producers. In addition to hydrodynamic processes

608   of remobilization from sediments and upstream inputs, other organisms such as zoo-plankton, zoo-

609   benthos, and especially bacteria could contribute significantly to the S-EPS pool. Further studies are

610   therefore needed to understand the origin of the S-EPS in highly hydrodynamic estuaries.

611

612   **5. Conclusion**

High frequency analysis of the photosynthetic parameters of phytoplankton revealed the presence of living cells with good physiological status in the bottom water layers pointing to a role for this fraction in the autochthonous production of this estuary. This finding has major implications for trophic transfer between pelagic and benthic organisms, which plays a key role in the nursery and feeding function of these ecosystems.

We also showed that EPS are not only linked to primary production processes but rather to stress levels (salinity, turbidity, temperature or hydrodynamics), demonstrating that healthy phytoplankton produce less EPS than stressed or senescent cells. EPS distributions especially TEP are thus mainly linked to hydrodynamic processes such as MTZ formation or sediment resuspension. Our estimation of the relative contribution of primary producers (phytoplankton and microphytobenthos) to S-EPS production show that the mudflats contribute less than 6% to the S-EPS pool in the water column, while phytoplankton produce up to 33%. The origin of a large proportion of the S-EPS in the water column thus remains unknown and further investigation is needed into potential secondary production of S-EPS by zoobenthos, zooplankton and heterotrophic microbial communities.

References

Adolf, J. E., C. L. Yeager, W. D. Miller, M. E. Mallonee, and L. W. Harding. 2006. Environmental forcing of phytoplankton floral composition, biomass, and primary productivity in Chesapeake Bay, USA. Estuarine, Coastal and Shelf Science **67**: 108–122.

Alpine, A. E., and J. E. Cloern. 1992. Trophic interactions and direct fhysical effects control

fhytoplankton biomass and production in an estuary. Limnology and Oceanography **37**: 946–955.

Aminot, A., and R. Kérouel. 2004. Hydrologie des écosystèmes marins: paramètres et analyses, Editions Quae.

Aminot, A., and R. Kérouel. 2007. Dosage automatique des nutriments dans les eaux marines. Méthodes d'analyse en milieu marin

Annane, S., L. St-Amand, M. Starr, E. Pelletier, and G. A. Ferreyra. 2015. Contribution of transparent exopolymeric particles (TEP) to estuarine particulate organic carbon pool. Marine Ecology Progress Series **529**: 17–34.

Ayadi, H., O. Abid, J. Elloumi, A. Bouaïn, and T. Sime-Ngando. 2004. Structure of the phytoplankton communities in two lagoons of different salinity in the Sfax saltern (Tunisia). Journal of Plankton Research **26**: 669–679.

Azam, F., T. Fenchel, J. G. Field, J. S. Graf, M.-R. L. A, and Thingstad F. 1983. The Ecological Role of Water-Column Microbes in the Sea. Marine Ecology **10**: 257–263.

Bar-Zeev, E., U. Passow, S. Romero-Vargas Castrillón, and M. Elimelech. 2015. Transparent exopolymer particles: From aquatic environments and engineered systems to membrane biofouling. Environmental Science and Technology **49**: 691–707.

Barbier, E., and S. Hacker. 2011. The value of estuarine and coastal ecosystem services. Ecological Monographs **81**: 169–193.

Barranguet, C., and J. Kromkamp. 2000. Estimating primary production rates from photosynthetic electron transport in estuarine microphytobenthos. Marine Ecology Progress Series **204**: 39–52.

Beauvais, S., M. L. Pedrotti, E. Villa, and R. Lemée. 2003. Transparent exopolymer particle (TEP) dynamics in relation to trophic and hydrological conditions in the NW Mediterranean Sea. Marine Ecology Progress Series **262**: 97–109.

Bhaskar, P. V, and N. B. Bhosle. 2005. Microbial extracellular polymeric substances in marine biogeochemical processes. Current Science **88**.

Brenon, I., and P. Le Hir. 1999. Modelling the Turbidity Maximum in the Seine Estuary (France): Identification of Formation. 525–544.

De Brouwer, J. F. C., G. K. Ruddy, T. E. R. Jones, and L. J. Stal. 2002. Sorption of EPS to sediment particles and the effect on the rheology of sediment slurries. Biogeochemistry **61**: 57–71.

Cai, W.-J., M. Dai, Y. Wang, W. Zhai, T. Huang, S. Chen, F. Zhang, Z. Chen, and Z. Wang. 2004. The biogeochemistry of inorganic carbon and nutrients in the Pearl River estuary and the adjacent Northern South China Sea. Continental Shelf Research **24**: 1301–1319.

Campbell, D. A., V. Hurry, a K. Clarke, P. Gustafsson, and G. Oquist. 1998. Chlorophyll fluorescence analysis of cyanobacterial photosynthesis and acclimation. Microbiology and molecular biology reviews : MMBR **62**: 667–683.

Chiovitti, A., P. Molino, S. A. Crawford, R. Teng, T. Spurck, and R. Wetherbee. 2004. The glucans extracted with warm water from diatoms are mainly derived from intracellular chrysolaminaran and not extracellular polysaccharides. European Journal of Phycology **39**: 117–128.

Chowdhury, C., N. Majumder, and T. K. Jana. 2016. Seasonal distribution and correlates of transparent exopolymer particles (TEP) in the waters surrounding mangroves in the Sundarbans. Journal of Sea Research **112**: 65–74.

Claquin, P., J. C. Kromkamp, and V. Martin-Jezequel. 2004. Relationship between photosynthetic metabolism and cell cycle in a synchronized culture of the marine alga Cylindrotheca fusiformis (Bacillariophyceae). European Journal of Phycology **39**: 33–41.

Claquin, P., I. Probert, S. Lefebvre, and B. Veron. 2008. Effects of temperature on photosynthetic parameters and TEP production in eight species of marine microalgae. Aquatic Microbial Ecology **51**: 1–11.

Cloern, J. E. 1991. Tidal stirring and phytoplankton bloom dynamics in an estuary. Journal of Marine Research **49**: 203–221.

Cloern, J. E. 1996. Phytoplankton bloom dynamics in coastal ecosystems: A review with some general lessons from sustained investigation of San Francisco Bay, California. Reviews of Geophysics **34**: 127–168.

Cloern, J. E., B. E. Cole, R. L. J. Wong, and A. E. Alpine. 1985. Temporal dynamics of estuarine

phytoplankton: A case study of San Francisco Bay. Hydrobiologia **129**: 153–176.

Cloern, J. E., S. Q. Foster, and a. E. Kleckner. 2014. Phytoplankton primary production in the world's estuarine-coastal ecosystems. Biogeosciences **11**: 2477–2501.

Cloern, J. E., and A. D. Jassby. 2010. Patterns and Scales of Phytoplankton Variability in Estuarine–Coastal Ecosystems. Estuaries and coasts **33**: 230–241.

Corzo, A., J. A. Morillo, and S. Rodríguez. 2000. Production of transparent exopolymer particles (TEP) in cultures of Chaetoceros calcitrans under nitrogen limitation. Aquatic Microbial Ecology **23**: 63–72.

Corzo, A., S. Rodriguez-Galvez, L. Lubian, P. Sangra, A. Martinez, and J. A. Morillo. 2005. Spatial distribution of transparent exopolymer particles in the Bransfield Strait, Antarctica. Journal of Plankton Research **27**: 635–646.

Decho, A. W. 2000. Microbial biofilms in intertidal systems: an overview. Cont. Shelf Res. **20**: 1257–1273.

Desmit, X., J. P. Vanderborght, P. Regnier, and R. Wollast. 2005. Control of phytoplankton production by physical forcing in a strongly tidal, well-mixed estuary. Biogeosciences Discussions **2**: 37–75.

Dubois, M., K. A. Gilles, J. K. Hamilton, Pa. Rebers, and F. Smith. 1956. Colorimetric method for determination of sugars and related substances. Analytical chemistry **28**: 350–356.

Eilers, P. H. C., and J. C. H. Peeters. 1988. A model for the relationship between light intensity and the rate of photosynthesis in phytoplankton. Ecological Modelling **42**: 199–215.

Engel, A. 2000. The role of transparent exopolymer particles (TEP) in the increase in apparent particle stickiness (alpha) during the decline of a diatom bloom. Journal of Plankton Research **22**: 485–497.

Engel, A., and U. Passow. 2001. Carbon and nitrogen content of transparent exopolymer particles (TEP) in relation to their Alcian Blue adsorption. Marine Ecology Progress Series **219**: 1–10.

Etcheber, H., A. Taillez, G. Abril, J. Garnier, P. Servais, F. Moatar, and M. V. Commarieu. 2007. Particulate organic carbon in the estuarine turbidity maxima of the Gironde, Loire and Seine estuaries: Origin and lability. Hydrobiologia **588**: 245–259.

Even, S., J. M. Mouchel, P. Servais, N. Flipo, M. Poulin, S. Blanc, M. Chabanel, and C. Paffoni. 2007. Modelling the impacts of Combined Sewer Overflows on the river Seine water quality. Science of the Total Environment **375**: 140–151.

Fukao, T., K. Kimoto, T. Yamatogi, K. I. Yamamoto, Y. Yoshida, and Y. Kotani. 2009. Marine mucilage in Ariake Sound, Japan, is composed of transparent exopolymer particles produced by the diatom Coscinodiscus granii. Fisheries Science **75**: 1007–1014.

Gameiro, C., and V. Brotas. 2010. Patterns of Phytoplankton variability in the Tagus estuary (Portugal). Estuaries and Coasts **33**: 311–323.

Garcia, C. M. 2002. Hydrodynamics and the spatial distribution of plankton and TEP in the Gulf of Cadiz (SW Iberian Peninsula). Journal of Plankton Research **24**: 817–833.

Garnier, J., G. Billen, J. Némery, and M. Sebilo. 2010. Transformations of nutrients (N, P, Si) in the turbidity maximum zone of the Seine estuary and export to the sea. Estuarine, Coastal and Shelf Science **90**: 129–141.

Genty, B., J. Harbinson, J. Briantais, N. R. Baker, and C. Lane. 1989. The relationship between non-photochemical quenching of chlorophyll fluorescence and the rate of photosystem 2 photochemistry in leaves. Photosynthesis research **25**: 249–257.

Glover, H. E., D. A. Phinney, and C. S. Yentsch. 1985. Photosynthetic characteristics of picoplankton compared with those of larger phytoplankton populations, in various water masses in the Gulf of Maine. Deep Sea Research Part B. Oceanographic Literature Review **32**: 759.

Goto, N., T. Kawamura, O. Mitamura, and H. Terai. 1999. Importance of extracellular organic carbon production in the total primary production by tidal-flat diatoms in comparison to phytoplankton. Marine Ecology Progress Series **190**: 289–295.

Heip, C. H. R., N. K. Goosen, P. M. J. Herman, J. Kromkamp, J. J. Middelburg, and K. Soetaert. 1995. Production and consumption of biological particles in temperate tidal estuaries,.

Hernando, M., I. R. Schloss, G. Malanga, G. O. Almandoz, G. A. Ferreyra, M. B. Aguiar, and S. Puntarulo. 2015. Effects of salinity changes on coastal Antarctic phytoplankton physiology and

748   assemblage composition. Journal of Experimental Marine Biology and Ecology **466**: 110–119.

749 Higgins, T. G. O., S. P. Ferraro, D. D. Dantin, and S. J. Jordan. 2010. Habitat Scale Mapping of
750   Fisheries Ecosystem Service Values in. Ecology and Society **15(4)**.

751 Le Hir, P., A. Ficht, R. S. Jacinto, P. Lesueur, J.-P. Dupont, R. Lafite, I. Brenon, B. Thouvenin, and P.
752   Cugier. 2001. Fine Sediment Transport and Accumulations at the Mouth of the Seine Estuary
753   (France). Estuaries **24**: 950.

754 Hong, Y. 1997. Studies on Transparent Exopolymer Particles (Tep) Produced in the Ross Sea
755   (Antarctica) and By Phaeocystis Antarctica (Prymnesiophyceae). **376**: 368–376.

756 Hydes, D., M. Aoyama, A. Aminot, K. Bakker, S. Becker, S. Coverly, A. Daniel, A. G. Dickson, O.
757   Grosso, R. Kerouel, J. van Ooijen, K. Sato, T. Tanhua, E. M. S. Woodward, and J. Z. Zhang. 2010.
758   Determination of dissolved nutrients (N, P, Si) in seawater with high precision and inter-
759   comparability using gas-segmented continuous flow analysers. The GO-SHIP Repeat Hydrography
760   Manual IOCCP Report **134**: 1–87.

761 Josselyn, M. N., and J. A. West. 1985. Temporal Dynamics of an Estuary: San Francisco Bay, p. 139–
762   152. *In* J.E. Cloern and F.H. Nichols [eds.]. Springer Netherlands.

763 Jouenne, F., S. Lefebvre, B. Véron, and Y. Lagadeuc. 2007. Phytoplankton community structure and
764   primary production in small intertidal estuarine-bay ecosystem (eastern English Channel, France).
765   Marine Biology **151**: 805–825.

766 Juneau, P., and P. J. Harrison. 2005. Comparison by PAM Fluorometry of Photosynthetic Activity of
767   Nine Marine Phytoplankton Grown Under Identical Conditions. photochemistry and photobiology
768   649–653.

769 Kaiser, M. J. 2011. Marine ecology: processes, systems, and impacts, Oxford University Press.

770 Klein, C., P. Claquin, P. Alexandrine, C. Napoléon, B. Le Roy, and B. Véron. 2011. Dynamics of
771   soluble extracellular polymeric substances and transparent exopolymer particle pools in coastal
772   ecosystems. Marine Ecology Progress Series **427**: 13–27.

773 Kolber, Z., and P. G. Falkowski. 1993. Use of active fluorescence to estimate phytoplankton
774   photosynthesis in situ. Limnology and Oceanography **38**: 1646–1665.

775 Kromkamp, J. C., and R. M. Forster. 2003. The use of variable fluorescence measurements in aquatic
776   ecosystems : differences between multiple and single turnover measuring protocols and suggested
777   terminology. European Journal of Phycology **38**: 103–112.

778 Kromkamp, J., J. Peene, P. van Rijswijk, A. Sandee, and N. Goosen. 1995. Nutrients, light and primary
779   production by phytoplankton and microphytobenthos in the eutrophic, turbid Westerschelde
780   estuary (The Netherlands). Hydrobiologia **311**: 9–19.

781 Lehman, P. W. 2007. The influence of phytoplankton community composition on primary productivity
782   along the riverine to freshwater tidal continuum in the San Joaquin River, California. Estuaries and
783   Coasts **30**: 82–93.

784 Lionard, M., K. Muylaert, D. Van Gansbeke, and W. Vyverman. 2005. Influence of changes in salinity
785   and light intensity on growth of phytoplankton communities from the Schelde river and estuary
786   (Belgium/The Netherlands). Hydrobiologia **540**: 105–115.

787 Liu, H., and E. J. Buskey. 2000. Hypersalinity Enhances the Production of Extracellular Polymeric.
788   Production **77**: 71–77.

789 Lorenzen, C. J. 1966. A method for the continuous measurement of in vivo chlorophyll concentration.
790   Deep Sea Research and Oceanographic Abstracts **13**: 223–227.

791 Macintyre, H. L., T. M. Kana, T. Anning, and R. J. Geider. 2002. Review Photoacclimatation of
792   photosynthesis Irradiance response curves and photosynthetic pigments in microalgae and
793   cyanobacteria. Journal of Phycology **38**: 17–38.

794 Malpezzi, M. A., L. P. Sanford, and B. C. Crump. 2013. Abundance and distribution of transparent
795   exopolymer particles in the estuarine turbidity maximum of Chesapeake Bay. Marine Ecology
796   Progress Series **486**: 23–35.

797 Masojidek, J., J. Grobbelaar, L. Pechar, and M. Koblizek. 2001. Photosystem II electron transport rates
798   and oxygen production in natural waterblooms of freshwater cyanobacteria during a diel cycle.
799   Journal of Plankton Research **23**: 57–66.

800 Middelburg, J. J., and P. M. J. Herman. 2007. Organic matter processing in tidal estuaries. Marine

Chemistry **106**: 127–147. ACCEPTED MANUSCRIPT

Monbet, Y. 1992. Control of Phytoplankton Biomass in Estuaries: A Comparative Analysis of Microtidal and Macrotidal Estuaries. Estuaries **15**: 563.

Morse, R. E., M. R. Mulholland, T. A. Egerton, and H. G. Marshall. 2014. Phytoplankton and nutrient dynamics in a tidally dominated eutrophic estuary: Daily variability and controls on bloom formation. Marine Ecology Progress Series **503**: 59–74.

Muylaert, K., K. Sabbe, and W. Vyverman. 2009. Changes in phytoplankton diversity and community composition along the salinity gradient of the Schelde estuary (Belgium/The Netherlands). Estuarine, Coastal and Shelf Science **82**: 335–340.

Napoleon, C., V. Raimbault, L. Fiant, P. Riou, S. Lefebvre, L. Lampert, and P. Claquin. 2012. Spatiotemporal dynamics of physicochemical and photosynthetic parameters in the central English Channel. Journal of Sea Research **69**: 43–52.

Némery, J., and J. Garnier. 2007. Origin and fate of phosphorus in the Seine watershed (France): Agricultural and hydrographic P budgets. Journal of Geophysical Research: Biogeosciences **112**: 1–14.

Orvain, F., M. De Crignis, K. Guizien, S. Lefebvre, C. Mallet, E. Takahashi, and C. Dupuy. 2014. Tidal and seasonal effects on the short-term temporal patterns of bacteria, microphytobenthos and exopolymers in natural intertidal biofilms (Brouage, France). Journal of Sea Research , doi:10.1016/j.seares.2014.02.018

Parizzi, R. A., E. Da, C. Machado, C. Prestes, D. Santos, L. F. Fernandes, M. G. De Camargo, L. Laureno, and M. Jr. 2016. Primary productivity and phytoplankton dynamics in a subtropical estuary : a multiple timescale approach. Scientia Marina **80**: 1–13.

Passow, U. 2002. Transparent exopolymer particles (TEP) in aquatic environments. Progress in Oceanography **55**: 287–333.

Passow, U., and A. L. Alldredge. 1995. A dye-binding assay for the spectrophotometric measurement of transparent exopolymer particles (TEP). Limnology and Oceanography **40**: 1326–1335.

Passow, U., R. F. Shipe, A. Murray, D. K. Pak, M. A. Brzezinski, and A. L. Alldredge. 2001. The origin of transparent exopolymer particles (TEP) and their role in the sedimentation of particulate matter. Continental Shelf Research **21**: 327–346.

Passy, P., R. Le Gendre, J. Garnier, P. Cugier, J. Callens, F. Paris, G. Billen, P. Riou, and E. Romero. 2016. Eutrophication modelling chain for improved management strategies to prevent algal blooms in the Bay of Seine. Marine Ecology Progress Series **543**: 107–125.

Pedrotti, M. L., F. Peters, S. Beauvais, M. Vidal, J. Egge, A. Jacobsen, and C. Marrasé. 2010. Effects of nutrients and turbulence on the production of transparent exopolymer particles: A mesocosm study. Marine Ecology Progress Series **419**: 57–69.

Porter, E. M., W. D. Bowman, C. M. Clark, J. E. Compton, L. H. Pardo, and J. L. Soong. 2013. Interactive effects of anthropogenic nitrogen enrichment and climate change on terrestrial and aquatic biodiversity. Biogeochemistry **114**: 93–120.

Radić, T., R. Kraus, D. Fuks, J. Radić, and O. Pečar. 2005. Transparent exopolymeric particles' distribution in the northern Adriatic and their relation to microphytoplankton biomass and composition. Science of the Total Environment **353**: 151–161.

Sarma, V., S. N. M. Gupta, P. V. R. Babu, T. Acharya, N. Harikrishnachari, K. Vishnuvardhan, N. S. Rao, N. P. C. Reddy, V. V Sarma, and Y. Sadhuram. 2009. Influence of river discharge on plankton metabolic rates in the tropical monsoon driven Godavari estuary, India. Estuarine, Coastal and Shelf Science **85**: 515–524.

Schreiber, U., U. Schliwa, and W. Bilger. 1986. Continuous recording of photochemical and non-photochemical chlorophyll fluorescence quenching with a new type of modulation fluorometer. Photosynthesis research **10**: 51–62.

Servais, P., and J. Garnier. 2006. Organic carbon and bacterial heterotrophic activity in the maximum turbidity zone of the Seine estuary (France). Aquatic Sciences **68**: 78–85.

Shaffer, G. P., and C. P. Onuf. 1985. Reducing the error in estimating annual production of benthic microflora: Hourly to monthly rates, patchiness in space and time. Marine Ecology Progress Series **26**: 221–231.

Statham, P. J. 2012. Nutrients in estuaries - An overview and the potential impacts of climate change. Science of the Total Environment **434**: 213–227.

Suggett, D. J., H. L. MacIntyre, and R. J. Geider. 2004. Evaluation of biophysical and optical determinations of light absorption by photosystem II in phytoplankton. Limnology and Oceanography: Methods **2**: 316–332.

Sun, C., Y. Wang, Q. P. Li, W. Yue, Y. Wang, F. Sun, and Y. Peng. 2012. Distribution characteristics of transparent exopolymer particles in the Pearl River estuary , China. **117**: 1–12.

Takahashi, E., J. Ledauphin, D. Goux, and F. Orvain. 2009. Optimising extraction of extracellular polymeric substances (EPS) from benthic diatoms: comparison of the efficiency of six EPS extraction methods. Marine and Freshwater Research **60**: 1201–1210.

Thornton, D. 2002. Diatom aggregation in the sea: mechanisms and ecological implications. European Journal of Phycology **37**: 149–161.

Underwood, G. J. C., and J. Kromkamp. 1999. Primary Production by Phytoplankton and Microphytobenthos in Estuaries. Advances in Ecological Research **29**: 93–153.

Underwood, G. J. C., D. M. Paterson, and R. J. Parkes. 1995. The measurement of microbial carbohydrate exopolymers from intertidal sediments. Limnol. Oceanogr **40**: 1243–1253.

Verney, R., R. Lafite, and J. C. Brun-Cottan. 2009. Flocculation potential of estuarine particles: The importance of environmental factors and of the spatial and seasonal variability of suspended particulate matter. Estuaries and Coasts **32**: 678–693.

Viles, H., and T. Spencer. 1995. Coastal Problems: Geomorphology, Ecology and Society at the coast, Edward Arn.

Villacorte, L. O., Y. Ekowati, H. N. Calix-Ponce, J. C. Schippers, G. L. Amy, and M. D. Kennedy. 2015. Improved method for measuring transparent exopolymer particles (TEP) and their precursors infresh and saline water. Water Research **70**: 300–312.

Wang, Z. B., M. C. J. L. Jeuken, H. Gerritsen, H. J. De Vriend, and B. A. Kornman. 2002. Morphology and asymmetry of the vertical tide in the Westerschelde estuary. Continental Shelf Research **22**: 2599–2609.

Wetz, M. S., M. C. Robbins, and H. W. Paerl. 2009. Transparent exopolymer particles (TEP) in a river-dominated estuary: Spatial-temporal distributions and an assessment of controls upon TEP formation. Estuaries and Coasts **32**: 447–455.

Wolfstein, K., J. F. C. De Brouwer, and L. J. Stal. 2002. Biochemical partitioning of photosynthetically fixed carbon by benthic diatoms during short-term incubations at different irradiances. Marine Ecology Progress Series **245**: 21–31.

Wotton, R. S. 2004. The essential role of exopolymers (EPS) in aquatic systems. Oceanography and marine biology: an annual review **42**: 57–94.

Wurl, O., and M. Holmes. 2008. The gelatinous nature of the sea-surface microlayer. Marine Chemistry **110**: 89–97.

893 **Figures**
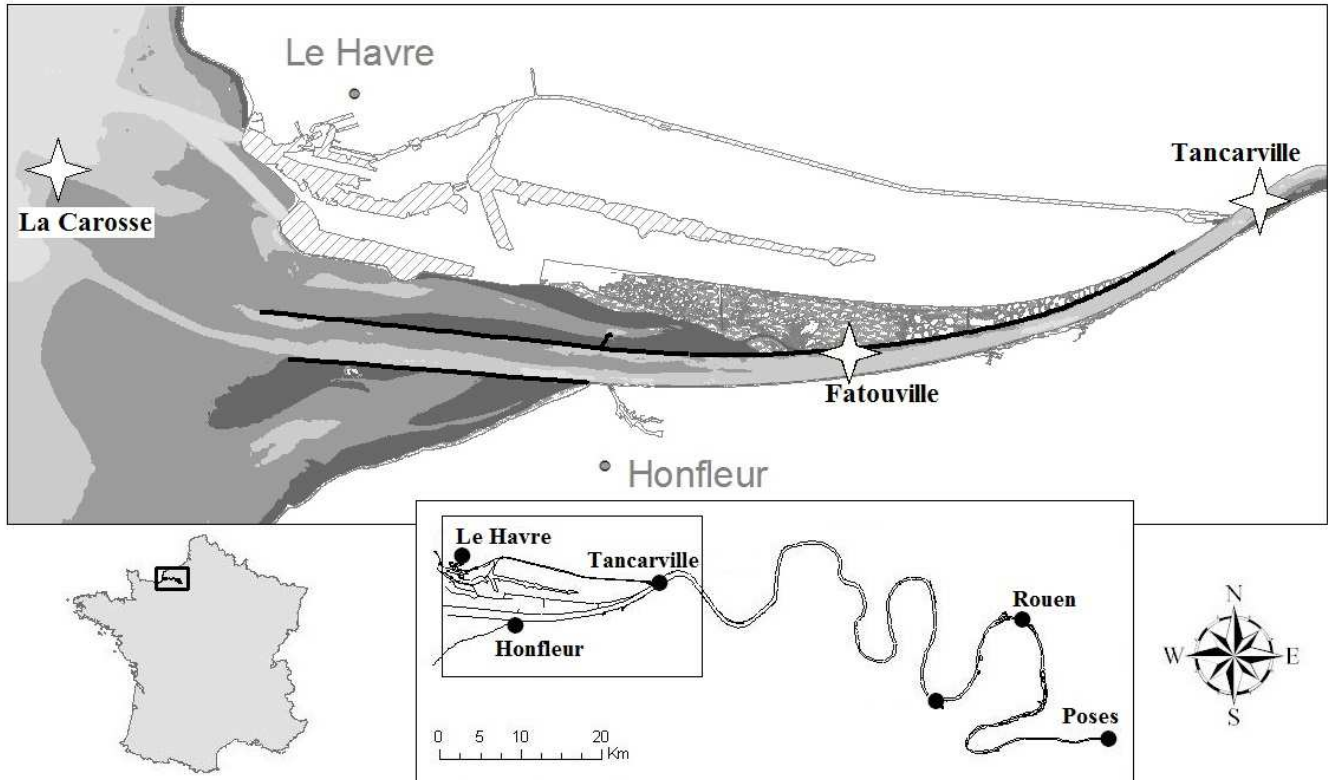
894
895 **Figure 1. Study area, the Seine Estuary, Normandy, France (49°26′09″N; 0°16′28″E).** Location of the 3 sampling sites
896 (white stars): (i) La Carosse (49°28'985"N; 0°01'807"E), located in the euhaline zone and sampled on February 3 and July
897 18, (ii) Fatouville (49°26'202"N; 0°19'274"E), located in the polyhaline zone and sampled on February 4 and July 20, (iii)
898 Tancarville (49°24'444"N; 0°28'200"E), located in the oligohaline zone and sampled on February 5 and July. Black dots
899 represent major cities along the Seine Estuary.

900

901
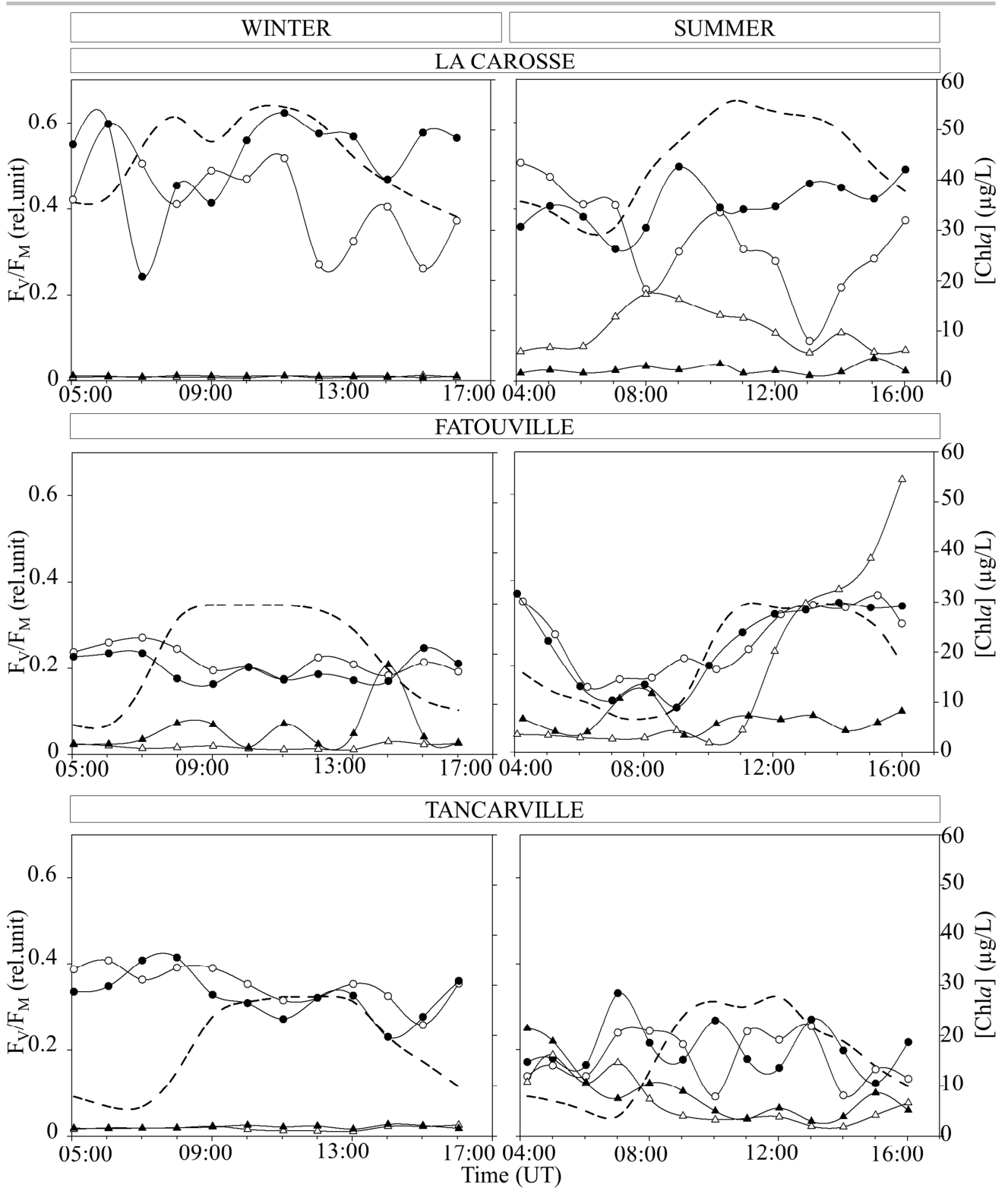
Figure 2. Phytoplankton biomass ([chl*a*], µg/L - triangles) **and** F_V/F_M (relative units - circles) **measured over a tidal cycle at the three sampling sites** (La Carosse, Fatouville and Tancarville), **in winter** (left panel) **and in summer** (right panel). Values measured 1 m below the surface are represented by empty circles and values measured 1 m above the water sediment interface (WSI) by black dots. The dashed lines represent tidal height (m) measured 1 m above the WSI (cf. Fig. 3).

902
903
904
905
906
907
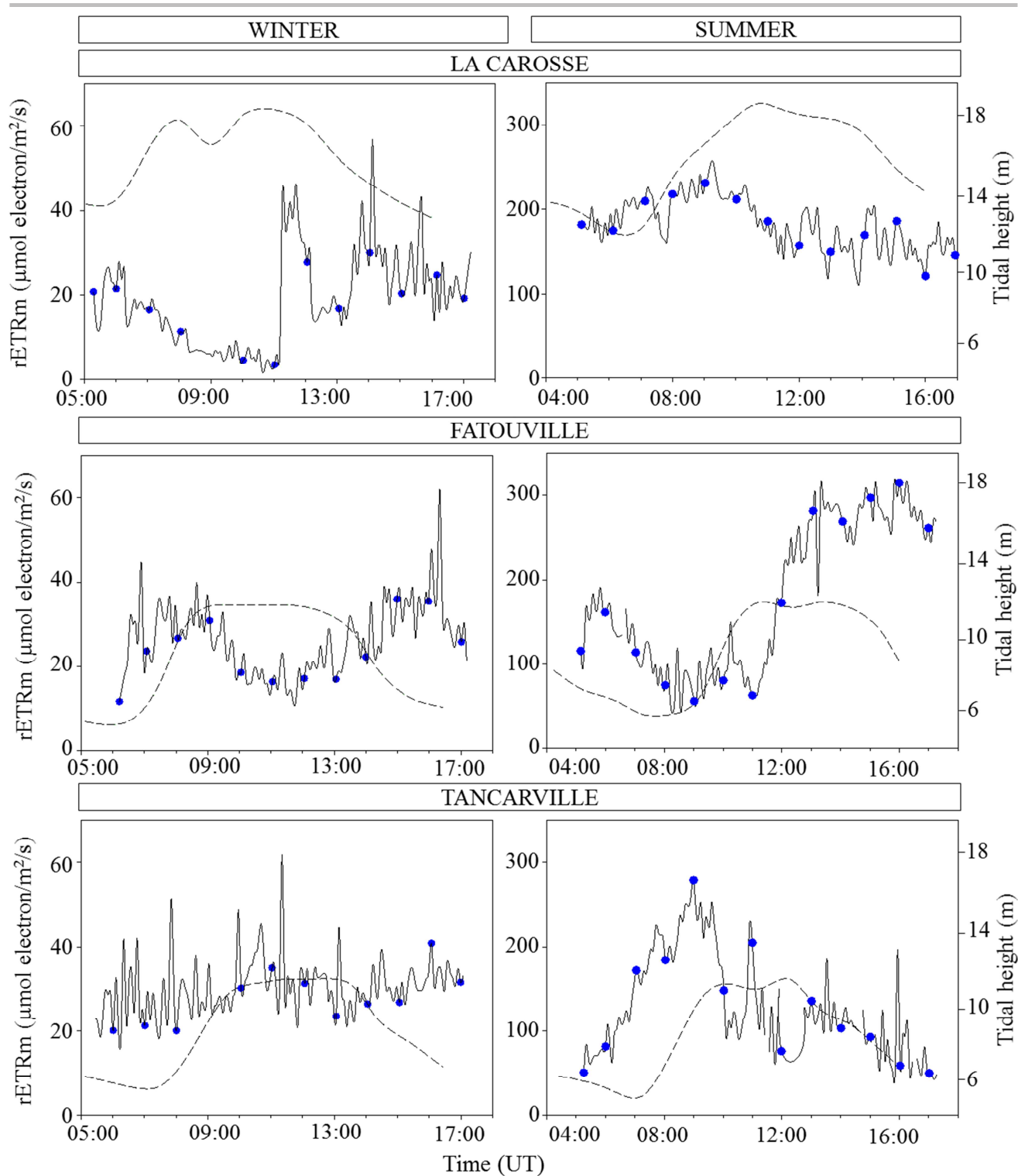
Figure 3. High frequency measurements of the maximum rate of electron transport (rETR$_{max}$; µmol electron/m^2/s – solid line) **measured over a tidal cycle at the three sampling sites** (La Carosse, Fatouville and Tancarville), **in winter** (left panel) **and in summer** (right panel). The dots represent values during low frequency sampling. The dashed lines represent tidal height (m) measured 1 m above the water sediment interface.
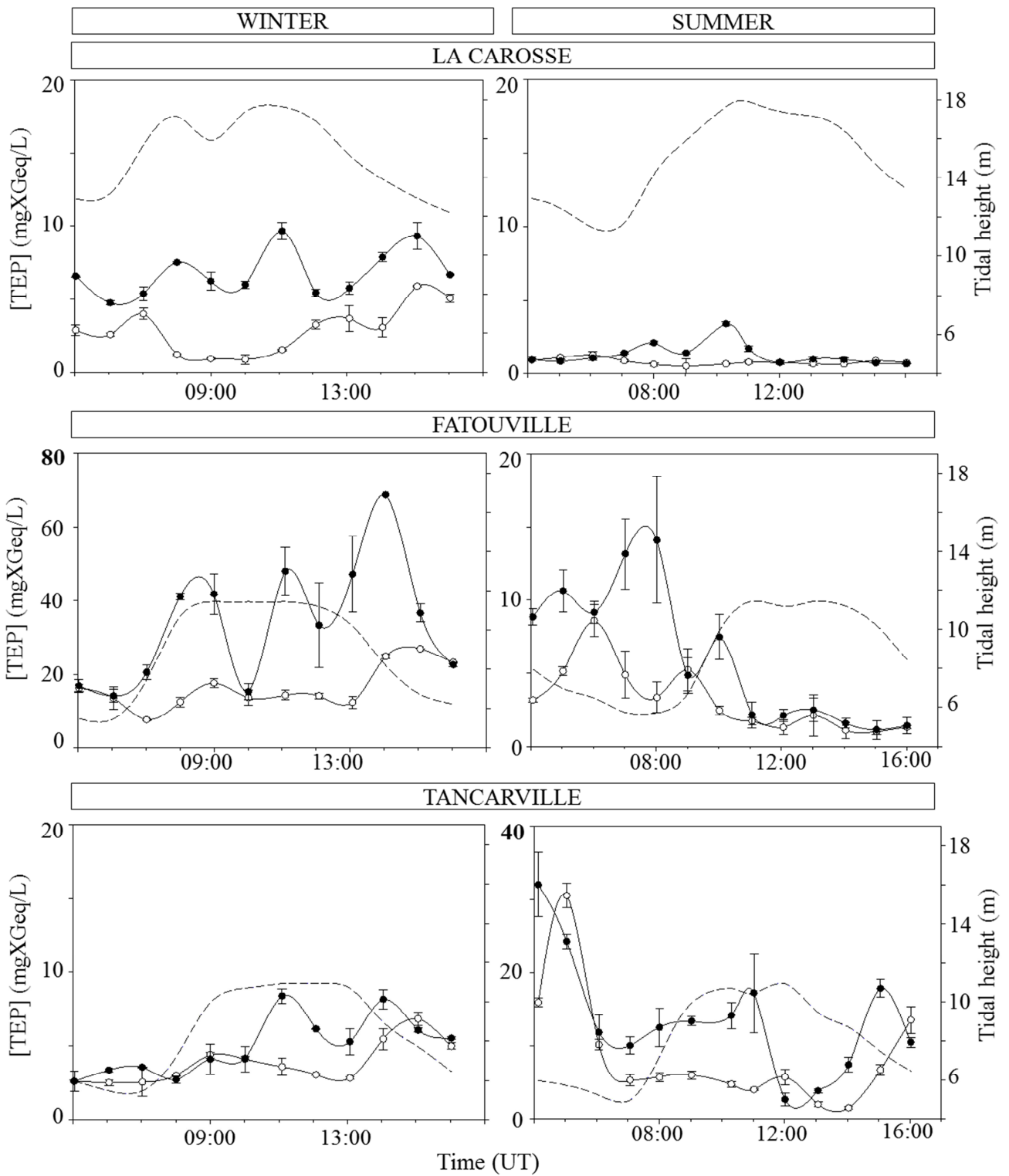
914
915 **Figure 4. Concentrations of transparent exopolymeric substances ([TEP]**; mgXGeq/L; mean ± standard error) **over a**
916 **tidal cycle at the three sampling sites** La Carosse, Fatouville & Tancarville, **in winter** (left panel) **and in summer** (right
917 panel). Values recorded 1 m below the surface are represented by empty circles and values measured 1 m above the WSI by
918 black dots. The dashed lines represent the tidal height (m).
919
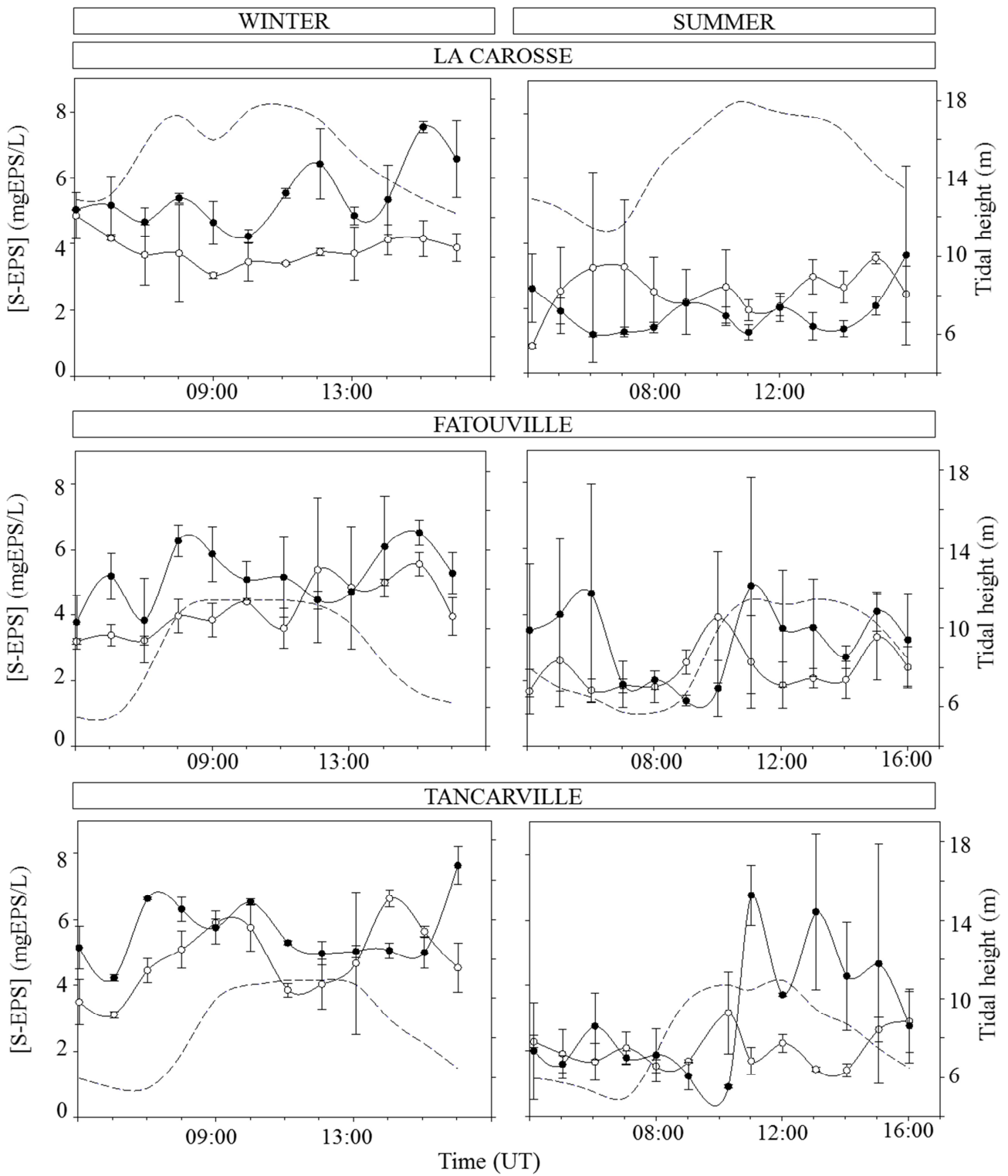
920
921 **Figure 5. Concentrations of soluble extracellular polymeric substances ([S-EPS]**; mgGeq/L*; mean ± standard error)
922 **over a tidal cycle at the three sampling sites** La Carosse, Fatouville & Tancarville, **in winter** (left panel) **and in summer**
923 (right panel). Values recorded 1 m below the surface are represented by empty circles and values measured 1 m above the
924 WSI by black dots. The dashed lines represent the tidal height (m).
925
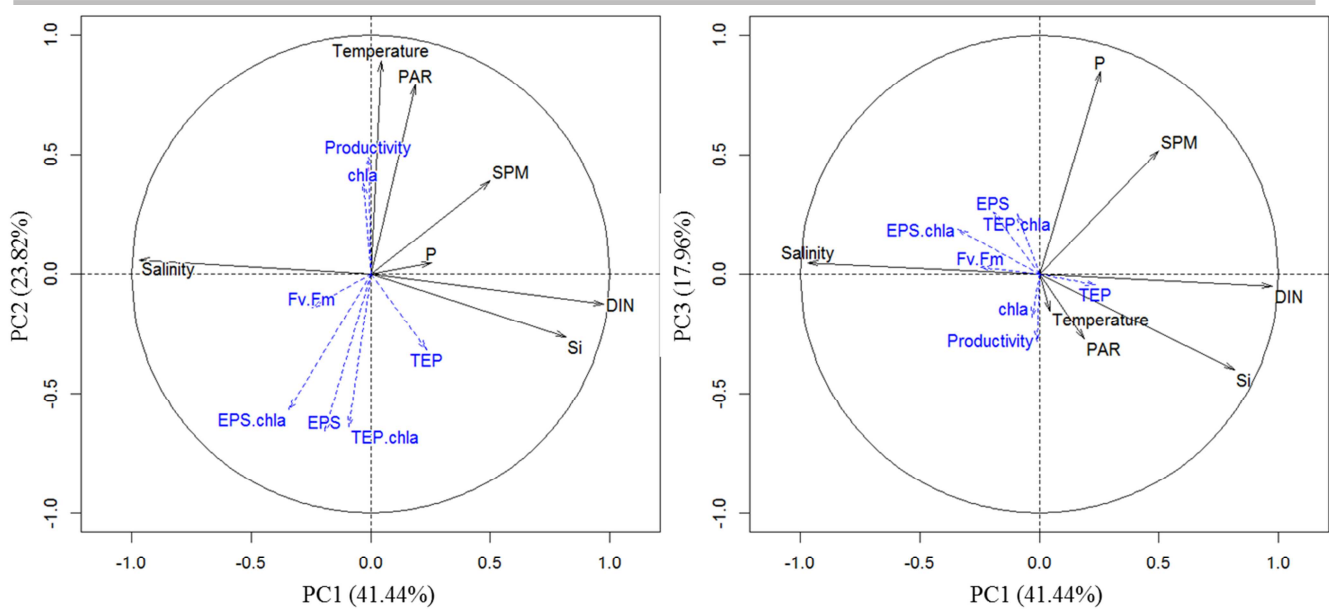
926
927 **Figure 6. Representation of Principal Component Analysis (PCA)** using the abiotic parameters (PAR (J/cm^2);
928 temperature (°C), salinity (PSU), SPM (g/L) and nutrients (µmol/L): DIN, P and Si) and as qualitative variables the
929 biological parameters (chl*a* (µg/L), F_V/F_M (rel.unit), Transparent exopolymeric particles (TEP) & exopolymeric substances
930 (EPS) concentrations (mgXGeq/L and mgEPS/L) and TEP & EPS per chl*a* unit (mgXGeq/mgchl*a* and mgEPS/mgchl*a*) as
931 quantitative variables. Dimensions 1 & 2 (65.26%) in the left panel and the dimensions 1 & 3 (59.40%) in the right panel.

932

933

Tables

Table 1. Minimum and maximum values of the sampling parameters recorded at each of the three sites (La Carosse (LC), Fatouville (Fat.) and Tancarville (Tan.)) in sub-surface (1 m below the surface (S)) and close to the bottom (1 m above the water sediment interface (B)) in February (winter) and in July (summer) 2015. The S-EPS concentrations are expressed in glucose equivalent (mgGeq) and the TEP concentrations in Xanthan gum equivalent (mgXGeq).

Sites	S/B	SPM g/L	Chl$a$ µg/L	F_V/F_M ratio	rETR$_{max}$ µmol electron/m²/s	TEP mgXGeq/L	TEP:Chl$a$ (x10³) mgXGeq/mgchl$a$	EPS mgGeq/L	EPS:Chl$a$ mgGeq/mgchl$a$
					Winter				
LC	S	0.01/0.11	0.49/1.01	0.26/0.60	3.52/29.95	0.87/5.90	1.46/8.00	3.06/4.85	3.66/8.14
	B	0.02/0.08	0.59/0.98	0.24/0.62	-	4.76/9.65	5.51/15.84	4.23/7.53	4.93/12.81
Fat.	S	0.03/1.77	0.97/2.55	0.18/0.27	11.69/47.82	7.57/26.94	6.22/14.33	3.20/5.56	1.51/4.99
	B	0.08/2.81	1.40/27.20	0.16/0.25	-	14.08/68.69	2.53/16.14	3.78/6.53	0.22/3.63
Tan.	S	0.03/0.22	1.00/2.27	0.26/0.41	20.11/40.87	2.52/6.82	1.50/3.42	3.10/6.64	1.84/4.69
	B	0.07/0.44	1.44/2.40	0.23/0.42	-	2.63/8.38	1.60/4.48	4.23/7.64	2.10/4.75
					Summer				
LC	S	0.00/0.02	5.71/17.37	0.09/0.51	120.81/231.03	0.52/1.27	0.03/0.18	0.85/3.54	0.13/0.60
	B	0.01/0.05	1.17/4.61	0.31/0.50	-	0.66/3.40	0.16/1.05	1.20/3.63	0.45/1.78
Fat.	S	0.02/0.43	1.84/54.57	0.15/0.37	55.84/314.65	1.00/8.58	0.02/2.99	1.67/3.92	0.04/8.59
	B	0.02/0.94	3.33/11.72	0.10/0.37	-	1.13/14.10	0.17/2.59	1.38/4.87	0.17/1.16
Tan.	S	0.03/1.03	1.80/16.12	0.09/0.25	49.56/278.75	1.53/30.59	0.37/2.06	1.42/5.15	0.12/1.30
	B	0.11/2.00	2.88/21.45	0.12/0.33	-	2.68/32.06	0.49/5.19	0.91/6.77	0.08/2.17

Table 2. Variations in mass of soluble extracellular polymeric substances per m² (mgEPS/m²) and in EPS:chl$a$ ratios (mgEPS/mgchl$a$) at the 15 sites sampled on the Seine estuary mudflats (Morelle *et al*, in prep.). The S-EPS concentrations are expressed in glucose equivalent (mgGeq) and the TEP concentrations in Xanthan gum equivalent (mgXGeq).

Site	Longitude (Wgs84)	Latitude (Wgs84)	September, 2014		April, 2015	
			EPS:chl$a$ (mgGeq/mgchl$a$)	EPS (mgGeq/m²)	EPS:chl$a$ (mgGeq/mgchl$a$)	EPS (mgGeq/m²)
O	0.2001	49.4267	1.33	87.10	33.52	149.82
C	0.2004	49.4482	33.91	480.45	NA	NA
N	0.1672	49.4162	10.78	377.18	33.78	284.73
E	0.2174	49.4483	1.55	264.12	4.31	91.02
P	0.2003	49.4235	5.83	197.33	92.56	149.01
B	0.2004	49.4506	5.45	409.84	11.62	227.14
F	0.2172	49.4462	6.95	437.90	4.99	129.03
H	0.2668	49.4408	7.19	181.99	36.78	118.06
G	0.267	49.4436	5.09	264.04	6.08	132.67
I	0.2668	49.4412	4.49	171.85	17.16	268.40
A	0.2004	49.4516	5.87	445.43	8.47	170.39
D	0.2174	49.4491	4.32	292.04	3.23	61.02
L	0.2836	49.4401	23.56	526.04	6.05	118.53
M	0.3003	49.4391	8.59	221.22	5.28	99.91
K	0.2836	49.4416	17.58	305.66	12.50	199.08
			9.50 ± 8.93	310.81 ± 129.61	19.74 ± 24.09	157.06 ± 66.16

Table 3. Eigenvalues, total variance and cumulative variance of the three factors of the principal component analysis.

Factor	I	II	III
Eigenvalues	2.90	1.67	1.26
Total variance (%)	41.44	23.82	17.96
Total variance (cumulative %)	41.44	65.26	83.22

948

949 **Title:** Dynamics of phytoplankton productivity and exopolysaccharide (EPS and TEP) pools in the

950 Seine Estuary (Normandy, France) over tidal cycles over two contrasting seasons.

951 **Authors:** Jérôme Morelle, Mathilde Schapira & Pascal Claquin

952 **Journal:** Marine Environmental Research

953

954 **Space and time dynamics of the water column along the salinity gradient**

955   At three different sites, in two seasons (winter & summer), and during a tide cycle, vertical salinity

956 (Practical Salinity Scale; Fig. S1) and temperature (°C; Fig. S1) profiles were performed hourly with a

957 SBE 19-plusVD CTD (Seabird) from the sub-surface down to 1 m above the water-sediment interface

958 (WSI). Water was sampled 1 m below the surface and 1 m above the WSI using a 5L-Niskin bottle at

959 hourly intervals to measure nutrients (µmol/L; Fig. S2), suspended particular matter (g/L; Fig. S3) and

960 biological parameters (chl*a*, TEP, S-EPS). TEP:chl*a* (mgXGeq/mgchl*a*; Fig. S4) and S-EPS:chl*a*

961 (mgGeq/mgchl*a*; Fig S5) were calculated. The principal values and dynamics of the parameters are

962 described in the main text.
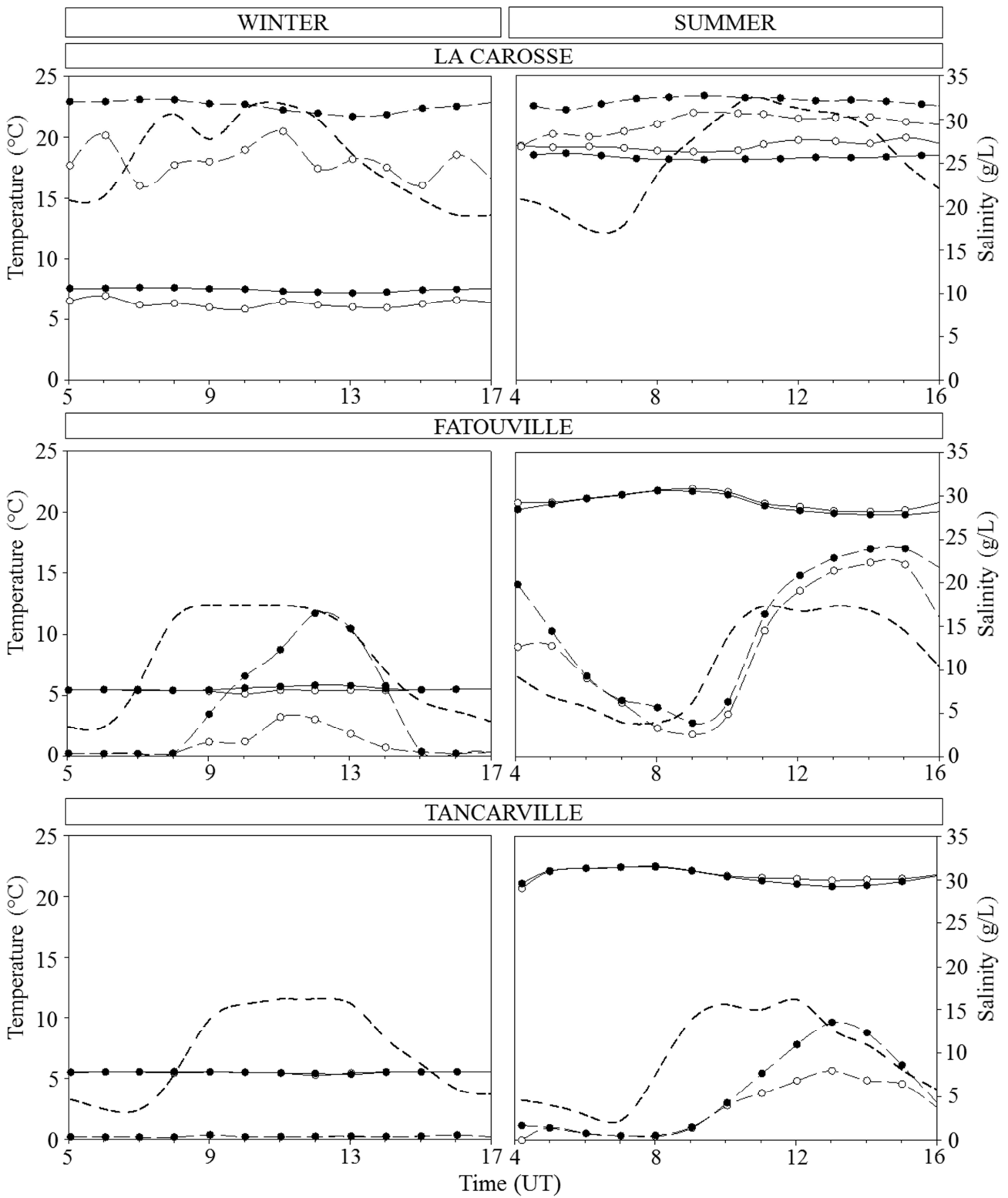
Figure S1. Temperature (°C; triangles) and salinity (circles) over a tidal cycle at the three sampling sites "La Carosse", "Fatouville" & "Tancarville", in winter (left panel) and in summer (right panel). Sub-surface (1 m) values are represented by empty symbols and values measured close to the bottom (1 m above the WSI) by black symbols. Dotted lines represent the tidal height (1 m above the WSI) *in the legend it should be* Time (UT)
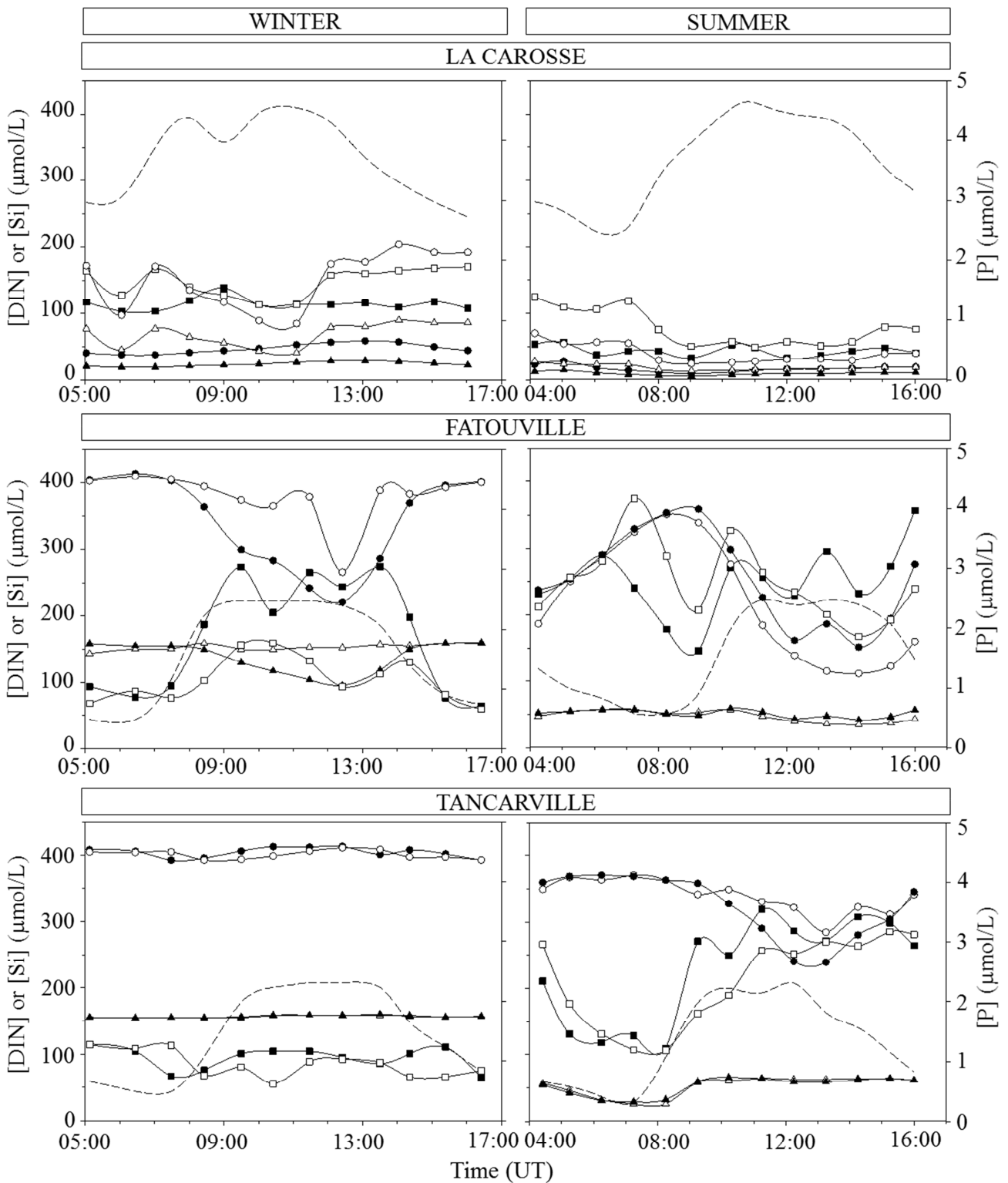
Figure S2. Nutrient dynamics (µmol/L) **with the dissolved inorganic nitrogen** (DIN=NO_3^-+NO_2^-+NH_4^+; circles), **phosphate** (PO_4^{3-}; squares) **and silicate** (Si(OH)$_4$; triangles) **measured over a tidal cycle at the three sampling sites (“**La Carosse”, “Fatouville” and “Tancarville”), **in winter** (left panel) **and in summer** (right panel). Sub-surface values (1 m below the surface) are represented by open symbols and values measured close to the bottom (1 m above the WSI) by black symbols. Dotted lines represent the tidal height (i.e.1 m above the WSI).
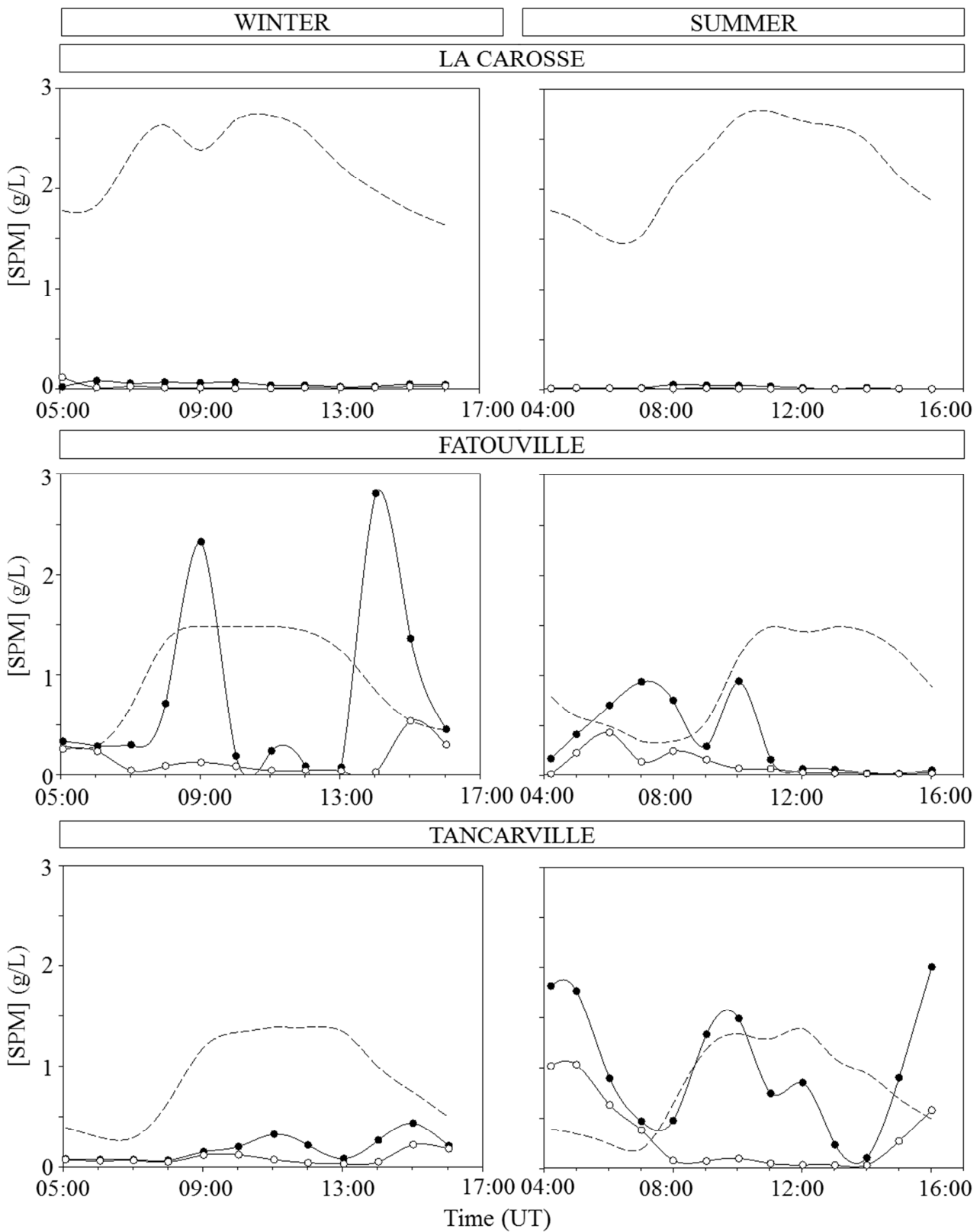
Figure S3. Suspended Particle Matter (SPM: g/L) **measured over a tidal cycle at the three sampling sites** (La Carosse, Fatouville and Tancarville), **in winter** (left panel) **and in summer** (right panel). Values recorded 1 m below the surface are represented by empty symbols and values measured close to the bottom (1 m above the water sediment interface) by black symbols. The dashed lines represent the tidal height (m).
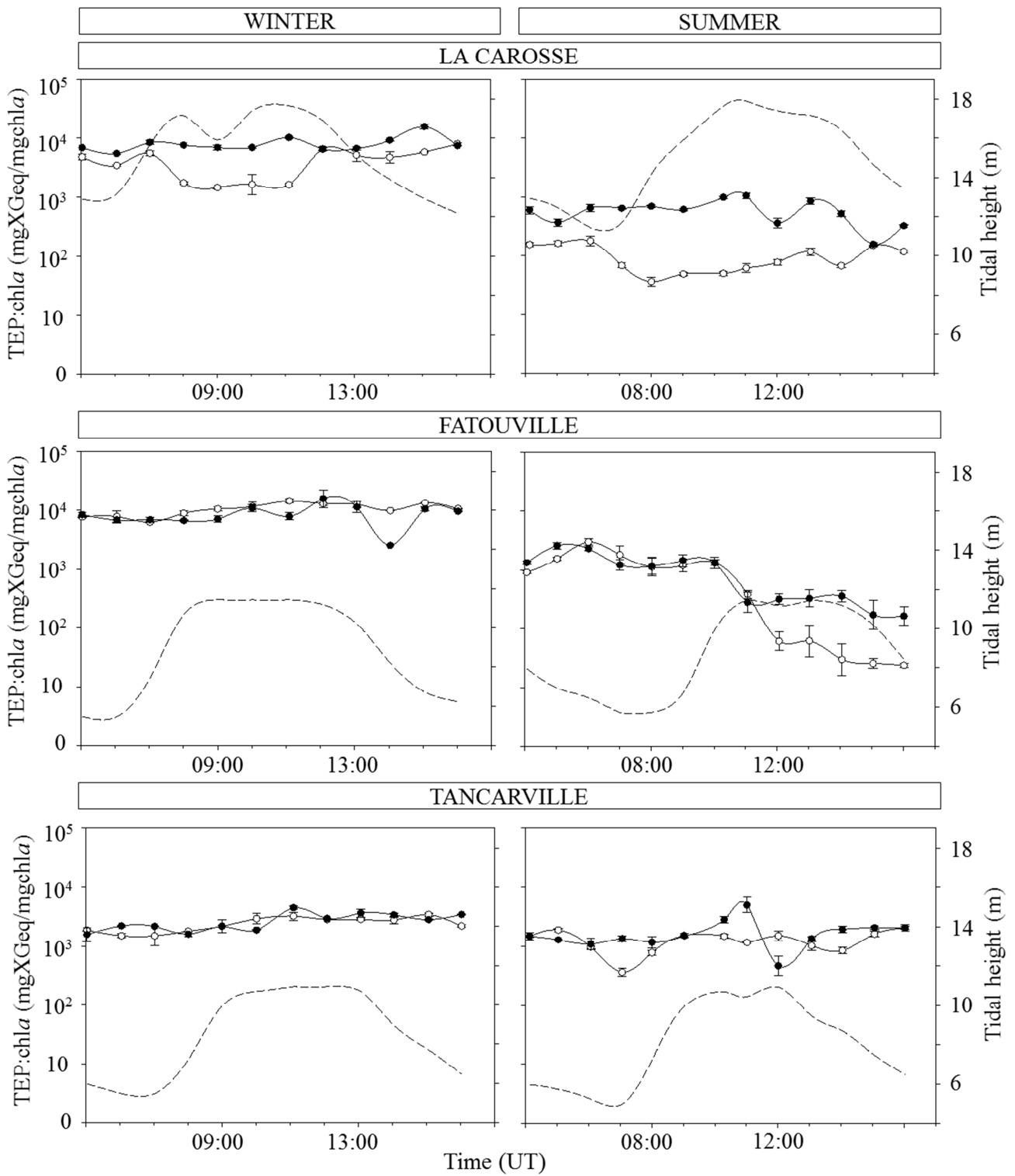
984
985 **Figure S4. TEP:chl*a* ratios** (mgXGeq/mg chl*a;* mean ± standard error) **over a tidal cycle at the three sampling sites
986 shown in logarithmic scale (log10)** La Carosse, Fatouville & Tancarville, **in winter** (left panel) **and in summer** (right
987 panel). Values recorded 1 m below the surface are represented by empty symbols and values measured 1 m above the WSI
988 by black symbols. The dashed lines represent the tidal height (m).

989
990
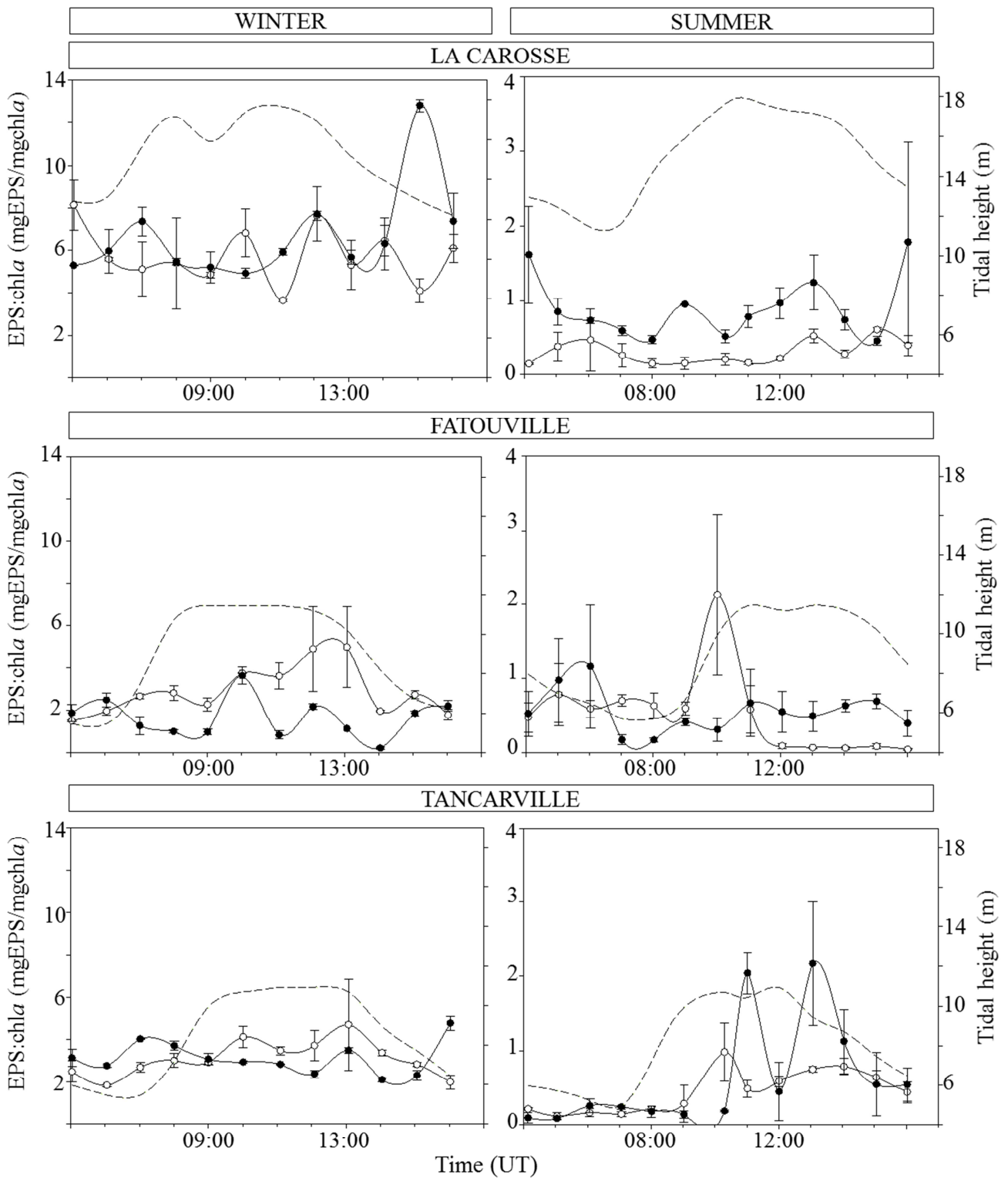
Figure S5. Variations in S-EPS:chl*a* ratios (mgGeq/mg chl*a;* mean ± standard error)) **over a tidal cycle at the three sampling sites** La Carosse, Fatouville & Tancarville, **in winter** (left panel) **and in summer** (right panel). Values recorded 1 m below the surface are represented by empty symbols and values measured 1 m above the WSI by black symbols. The dashed lines represent tidal height measured 1 m above the WSI.